

ASSESSING SPATIAL DISPARITIES: A BAYESIAN LINEAR REGRESSION APPROACH

KYLE LIN WU AND SUDIPTO BANERJEE

ABSTRACT. Epidemiological investigations of regionally aggregated spatial data often involve detecting spatial health disparities among neighboring regions on a map of disease mortality or incidence rates. Analyzing such data introduces spatial dependence among the health outcomes and seeks to report statistically significant spatial disparities by delineating boundaries that separate neighboring regions with disparate health outcomes. However, there are statistical challenges to appropriately defining what constitutes a spatial disparity and to construct robust probabilistic inference for spatial disparities. We enrich the familiar Bayesian linear regression framework to introduce spatial autoregression and offer model-based detection of spatial disparities. We derive exploitable analytical tractability that considerably accelerates computation. Simulation experiments conducted over a county map of the entire United States demonstrate the effectiveness of our method and we apply our method to a data set from the Institute of Health Metrics and Evaluation (IHME) on age-standardized US county-level estimates of lung cancer mortality rates.

1. INTRODUCTION

We develop statistical methods for detecting spatial disparities on maps. Disparities in health outcomes is a rapidly evolving field within public health (see, e.g., [Rao, 2023](#)) and spatial variation in health outcomes affects how disparities manifest on disease maps. Spatial data analysis in epidemiological investigations is extensively documented (see, e.g., [Lawson, 2013](#); [Lawson et al., 2016](#); [Waller and Carlin, 2010](#); [Waller and Gotway, 2004](#), and references therein). Inference on disparities proceeds from “difference boundaries” that represent significant differences among neighbors and delineate regions with significantly different disease mortality and incidence rates, which assists in improved geographic allocation of health care resources. In geographic analysis, the problem is often called “wombling” (see [Fitzpatrick et al., 2010](#); [Jacquez and Greiling, 2003a,b](#); [Li et al., 2011](#); [Lu and Carlin, 2005](#); [Ma and Carlin, 2007](#), for some algorithmic approaches with applications). Probabilistic model-based approaches include developments in [Corpas-Burgos and Martinez-Beneito \(2020\)](#); [Gao et al. \(2023\)](#); [Hanson et al. \(2015\)](#); [Lee and Mitchell \(2012\)](#); [Li et al. \(2012, 2015\)](#); [Lu et al. \(2007\)](#); [Ma et al. \(2010\)](#) and [Aiello and Banerjee \(2023\)](#).

While the aforementioned articles present an impressive range of methods, they are broadly classified into two groups. The first embraces hierarchical models and Bayesian inference for

the spatial adjacency matrix by modeling its elements. The second endows the spatial random effects with a probability law that accommodates nonzero probabilities on neighboring spatial random effects being equal (often using an areal Dirichlet process or some adaptation thereof), which are computed as posterior probabilities. Both groups introduce spatial dependence and aim to balance underlying spatial similarities with the ability to detect differences among neighbors. Our current contribution offers a computationally scalable and analytically tractable approach to this problem. Instead of modeling spatial effects as realizations of a Dirichlet process, which struggles to learn from the data and impedes convergence of iterative estimation algorithms, we devise fully model-based Bayesian inference within an augmented spatial linear regression framework. More specifically, we treat spatial disparities as a multiple comparison problem within a Bayesian inferential paradigm by testing for differences in spatial random effects between neighboring regions. Subsequently, we use posterior probabilities of such differences to detect spatial disparities while controlling a Bayesian false discovery rate or FDR (Müller et al., 2007). Benefits of our approach include clearer interpretation of spatial effects, computational simplicity, accounting for small differences in the values of neighboring spatial effects of adjacent regions in ascertaining spatial disparity, and delivering improved sensitivity and specificity for difference boundary detection (as seen in the analysis by Gao et al., 2023).

We exploit closed form distribution theory to account for the differences between the values of the spatial effects and evaluate posterior probabilities of such differences exceeding a certain threshold. We extend Lu and Carlin (2005) and Fitzpatrick et al. (2010), who use only posterior means or spatial residuals to detect differences, to fully model-based inference. We provide an outline for the rest of the article. Section 2 discusses the problem of detecting differences between fixed effects in a linear model before we extend to spatial random effects. Section 3 develops the notion of a difference boundary, demonstrates a meaningful connection to traditional hypothesis testing in the simple linear regression model, and considers extensions to a generalized linear model. Section 4 evaluates our methods using simulated data over a map of U.S. counties followed by an analysis of lung cancer mortality data in Section 5. Section 6 concludes with a brief discussion.

2. ASSESSING CONTRASTS IN BAYESIAN LINEAR REGRESSION

2.1. Random Effects under an Augmented Linear System. We follow Riebler et al. (2016) who adapted the “BYM” model (Besag et al., 1991) to ensure identifiable parameters and afford better interpretation. We write this “BYM2” model as

$$y = X\beta + \gamma + \eta, \quad \gamma = \sigma\sqrt{\rho}\phi, \quad \phi \sim N_n(0, V_\phi), \quad \eta = \sigma\sqrt{1-\rho}v, \quad v \sim N_n(0, I_n) \quad (1)$$

where ϕ is an $n \times 1$ vector of random effects, V_ϕ is a known positive definite matrix. For subsequent analysis, we specify a conditionally autoregressive (CAR) structure, $V_\phi^{-1} = c(D_W - \alpha W)$, where W is the adjacency matrix, D_W is diagonal with the diagonal elements $D_{W,ii}$ being the number of neighbors of region i , α is the spatial smoothing parameter, and c is a scaling factor. The parameter

σ^2 captures the overall error variance if c is set so that the geometric mean of the marginal prior variances is approximately one, and ρ represents the proportion of total variance attributed to the spatial structure (Riebler et al., 2016).

If $\pi(\gamma, \beta, \sigma^2, \rho) = N(\gamma | 0, \sigma^2 \rho V_\phi) \times N(\beta | M_0 m_0, \sigma^2 M_0) \times \text{IG}(\sigma^2 | a_{\sigma^2}, b_{\sigma^2}) \times \pi(\rho)$ is the prior for (1), then the joint distribution arises from the augmented linear model,

$$\underbrace{\begin{bmatrix} y \\ M_0 m_0 \\ 0_n \end{bmatrix}}_{y_\star} = \underbrace{\begin{bmatrix} X & I_n \\ I_p & 0_{p \times n} \\ 0_{n \times p} & I_n \end{bmatrix}}_{X_\star} \underbrace{\begin{bmatrix} \beta \\ \gamma \end{bmatrix}}_{\gamma_\star} + \underbrace{\begin{bmatrix} \eta \\ \eta_\beta \\ \eta_\phi \end{bmatrix}}_{\eta_\star}, \quad \eta_\star \sim N_{2n+p} \left(0_{2n+p}, \sigma^2 V_{y_\star} \right), \quad (2)$$

where $V_{y_\star} = \begin{bmatrix} (1-\rho)I_n & 0 & 0 \\ 0 & M_0 & 0 \\ 0 & 0 & \rho V_\phi \end{bmatrix}$ and a prior $\pi(\gamma_\star, \sigma^2, \rho) = \text{IG}(\sigma^2 | a_{\sigma^2}, b_{\sigma^2}) \times \pi(\rho)$ (since the prior for $\gamma_\star = (\beta^\top, \gamma^\top)^\top$ has been absorbed into the linear system). The resulting conditional posterior joint distribution, $\pi(\gamma_\star, \sigma^2 | y, \rho)$, is

$$\pi(\gamma_\star, \sigma^2 | y, \rho) = N_{n+p} \left(\gamma_\star | M_\star m_\star, \sigma^2 M_\star \right) \times \text{IG} \left(\sigma^2 | a_n, b_n \right), \quad (3)$$

where $M_\star = (X_\star^\top V_{y_\star}^{-1} X_\star)^{-1}$, $m_\star = X_\star^\top V_{y_\star}^{-1} y_\star = \left(\frac{1}{1-\rho} y^\top X + m_0^\top, \frac{1}{1-\rho} y^\top \right)^\top$, $a_n = a_{\sigma^2} + \frac{n}{2}$, and $b_n = b_{\sigma^2} + \frac{1}{2} \left(\frac{1}{1-\rho} y^\top y + m_0^\top M_0 m_0 - m_\star^\top M_\star m_\star \right)$. The posterior mean $M_\star m_\star = \hat{\gamma}_\star$ is the general least square regression estimate solving $X_\star^\top V_{y_\star}^{-1} X_\star \hat{\gamma}_\star = X_\star^\top V_{y_\star}^{-1} y_\star$ and $b_n = b_{\sigma^2} + \frac{ns^2}{2}$, where $s^2 = \frac{1}{n} (y_\star - X_\star \hat{\gamma}_\star)^\top V_{y_\star}^{-1} (y_\star - X_\star \hat{\gamma}_\star)$ is the mean residual sums of squares from (2).

If $\rho \in (0, 1)$ is fixed, then we can draw exact posterior samples from (3). Noting that $\gamma = \sigma \sqrt{\rho} \phi$ and carrying out some familiar linear algebra calculations, we obtain

$$\text{Var}(\phi | y, \sigma^2, \rho) = \left(V_\phi^{-1} + \frac{\rho}{1-\rho} \left(I_n - X A^{-1} X^\top \right) \right)^{-1}, \quad (4)$$

where $A = X^\top X + (1-\rho)M_0^{-1}$. A flat prior on β , i.e., $M_0^{-1} = O$, yields $A = X^\top X$ and

$$\lim_{M_0^{-1} \rightarrow O} \text{Var}(\phi | y, \sigma^2, \rho) = \left(V_\phi^{-1} + \frac{\rho}{1-\rho} (I_n - H) \right)^{-1}, \quad \text{where } H = X(X^\top X)^{-1} X^\top. \quad (5)$$

These expressions are used in Section 3.2 to formulate difference boundary detection.

2.2. Limiting cases. The limits of the conditional posterior distribution of (β, γ) as $\rho \rightarrow 0^+$ or as $\rho \rightarrow 1^-$ are analytically derived when the prior is non-informative on β . By the spectral decomposition, $V_\phi^{1/2} (I - H) V_\phi^{1/2} = C D C^\top$ where C is an orthogonal matrix and $D = \text{diag}(d_1, \dots, d_n)$ with entries that are the non-negative eigenvalues of $V_\phi^{1/2} (I - H) V_\phi^{1/2}$. Let $U = V_\phi^{1/2} C$, then U is invertible, $U^\top V_\phi^{-1} U = I_n$, $U^\top (I_n - H) U = D$, $\text{Var}(\gamma | y, \sigma^2, \rho) = \sigma^2 U \left(\frac{1}{\rho} I_n + \frac{1}{1-\rho} D \right)^{-1} U^\top$, and $\mathbb{E}[\gamma | y, \sigma^2, \rho] = U \left(\frac{1-\rho}{\rho} I_n + D \right)^{-1} D U^{-1} y$. Calculations reveal $\lim_{\rho \rightarrow 0^+} \text{Var}(\gamma | y, \sigma^2, \rho) = 0_{n \times n}$

and $\lim_{\rho \rightarrow 0^+} \mathbb{E}[\gamma | y, \sigma^2, \rho] = 0_n$. Therefore, if the prior on β is flat, then $\lim_{\rho \rightarrow 0^+} \pi(\beta, \gamma, \sigma^2 | y, \rho)$ collapses to the degenerate mass at $\gamma = 0_n$.

We also obtain $\lim_{\rho \rightarrow 1^-} \left(\frac{1}{\rho} I_n + \frac{1}{1-\rho} D \right)^{-1} = I_n - D^*$ and $\lim_{\rho \rightarrow 1^-} \left(\frac{1-\rho}{\rho} I_n + D \right)^{-1} D = D^*$ where $D^* \in \mathbb{R}^{n \times n}$ is diagonal with $D_{ii}^* = I(d_i > 0)$ for $i = 1, \dots, n$. Further simplifications reveal that $\mathbb{E}[\beta | y, \sigma^2, \rho] \rightarrow (X^T X)^{-1} X^T (y - U D^* U^{-1} e)$ and $\mathbb{E}[\gamma | y, \sigma^2, \rho] \rightarrow U D^* U^{-1} e$ as $\rho \rightarrow 1^-$, where $e = (I - H)y$. Furthermore, $\text{Var}(\beta | y, \sigma^2, \rho) \rightarrow \sigma^2 (X^T X)^{-1} X^T V X (X^T X)^{-1}$, $\text{Var}(\gamma | y, \sigma^2, \rho) \rightarrow \sigma^2 V$ and $\text{Cov}(\beta, \gamma | y, \sigma^2, \rho) \rightarrow -\sigma^2 (X^T X)^{-1} X^T V$ as $\rho \rightarrow 1^-$, where $V = V_\phi - U D^* U^T$. Finally, $\lim_{\rho \rightarrow 1^-} b_n = b_{\sigma^2} + \frac{1}{2} v^T D^* v$, where $v = U^{-1} e$ (see Section S4). Therefore, $\lim_{\rho \rightarrow 1^-} \pi(\sigma^2 | y, \rho) = \text{IG}(\sigma^2 | a_{\sigma^2} + n/2, b_{\sigma^2} + v^T D^* v/2)$. These limiting cases have implications for subsequent boundary detection (see Section 3.5).

3. A NEW FRAMEWORK FOR DETECTING SPATIAL DISPARITIES

3.1. Connection to Classical Hypothesis Testing. We first briefly address testing for contrasts in Bayesian linear regression without spatial effects, i.e., $\gamma = 0$ in (1). Whereas $\mathbb{P}(c_k^T \beta = 0 | y) = 0$ for a continuous posterior distribution, we can test $H_0^{(k)} : c_k^T \beta = 0$ against $H_1^{(k)} : c_k^T \beta \neq 0$ for K non-zero $p \times 1$ vectors c_1, \dots, c_K using a classical linear model, $y = X\beta + \eta, \eta \sim N_n(0_n, \sigma^2 V_y)$, where β is fixed but unknown (e.g., [Seber and Lee, 2003](#)). We compute $t_{\text{obs}}^{(k)} = \frac{c_k^T \hat{\beta}}{\hat{\sigma} \sqrt{c_k^T (X^T V_y^{-1} X)^{-1} c_k}}$ for each c_k , where $\hat{\beta} = (X^T V_y^{-1} X)^{-1} X^T V_y^{-1} y$ and $(n-p)\hat{\sigma}^2 = (y - X\hat{\beta})^T V_y^{-1} (y - X\hat{\beta})$ are the generalized least squares estimates. We reject $H_0^{(k)}$ if the p-values $p_k = \mathbb{P}(T > |t_{\text{obs}}^{(k)}|)$, where $T \sim t_{n-p}$, are below a multiplicity adjusted threshold.

For Bayesian inference, we retain the continuous conjugate prior on β and evaluate posterior probabilities for the absolute standardized linear combinations among elements of β to exceed a threshold ϵ . Hence, for all $k = 1, \dots, K$ and any $\epsilon > 0$, we define

$$v_k(\epsilon) = \mathbb{P} \left(\frac{|c_k^T \beta|}{\sigma \sqrt{c_k^T M c_k}} > \epsilon \mid y \right). \quad (6)$$

We refer to these posterior probabilities as ϵ -difference probabilities, where ϵ represents a universal threshold across all K linear combinations indicating the number of posterior standard deviation units that $|c_k^T \beta|$ is away from 0. If $\beta^{(1)}, \dots, \beta^{(N)}$ and $\sigma^{(1)}, \dots, \sigma^{(N)}$ are N samples drawn from their respective posterior distributions, then we estimate (6) using

$$\hat{v}_k(\epsilon) = \frac{1}{N} \sum_{t=1}^N \mathbb{I} \left(\frac{|c_k^T \beta^{(t)}|}{\sigma^{(t)} \sqrt{c_k^T M c_k}} > \epsilon \right) \quad (7)$$

for any given ϵ . Adapting (2) to $\gamma = 0$ yields $\pi(\beta, \sigma^2 | y) = N(\beta | Mm, \sigma^2 M) \times \text{IG}(\sigma^2 | a, b)$, where $a = a_0 + \frac{n}{2}$, $b = b_0 + \frac{1}{2} (y^T V_y^{-1} y + m_0^T M_0 m_0 - m^T M m)$, $M^{-1} = M_0^{-1} + X^T V_y^{-1} X$ and $m = m_0 + X^T V_y^{-1} y$.

We draw exact posterior samples from the Normal-Gamma family. Specific domain applications may provide further insights into possible constraints on ϵ and what is considered to be a clinically meaningful difference between coefficients β_i and β_j , which, for example, could represent mean outcomes for different treatment groups in a Bayesian Analysis Of Variance (ANOVA).

Classical p-values and the probabilities $\{v_k(\epsilon)\}_k$ defined in (6) have opposite interpretation: a small value of p_k suggests $|c_k^T \beta|$ is far from 0, while small $v_k(\epsilon)$ suggests $|c_k^T \beta|$ is likely to be close to 0. In fact, Bayesian inference with a flat prior on β amounts to using the classical generalized least squares estimate $\widehat{\beta}$. Hence, with a specific prior, the p-values and ϵ -difference probabilities yield identical decisions on contrasts in the following sense.

Theorem 1. *Let $c_1, \dots, c_K \in \mathbb{R}^p$, $X \in \mathbb{R}^{n \times p}$, $y \in \mathbb{R}^n$, and $V_y \in \mathbb{R}^{n \times n}$ be fixed. Under the standard linear model $y \sim N_n(X\beta, \sigma^2 V_y)$, let p_k be the p-value for testing the null hypothesis $H_0^{(k)} : c_k^T \beta = 0$ against $H_1^{(k)} : c_k^T \beta \neq 0$ for $k = 1, \dots, K$. Then, $p_k > p_{k'}$ if and only if $v_k(\epsilon) < v_{k'}(\epsilon)$ for all $k \neq k'$, where $v_k(\epsilon) = \mathbb{P} \left(\frac{|c_k^T \beta|}{\sigma \sqrt{c_k^T M c_k}} > \epsilon \mid y \right)$ under $\pi(\beta, \sigma^2) \propto \pi(\sigma^2)$.*

Proof. See Proof of Theorem 1.

Theorem 1 implies that the ascending order of the p-values associated with null hypotheses of the form $H_0^{(k)} : c_k^T \beta = 0$ with two-sided alternative $H_1^{(k)} : c_k^T \beta \neq 0$ is equivalent to the descending order of the Bayesian ϵ -difference probabilities. Since this result holds for all $\epsilon > 0$ and the classical procedure does not depend on ϵ , the Bayesian rankings are stable with respect to ϵ .

3.2. Extension to Spatial Random Effects. We consider (1), where each observation corresponds to one region. We let V_ϕ be known, whereas ρ can either be a fixed hyperparameter or a random variable with a prior density. Generalizing the ϵ -difference probabilities in the fixed effects model, we conduct posterior inference on random variables $r_k(\epsilon) = \mathbb{I} \left(\frac{|c_k^T \gamma_\star|}{\sigma \sqrt{c_k^T M_\star c_k}} > \epsilon \right)$ for any given $\epsilon > 0$. For $k = 1 \dots, K$, we define

$$h_k(\epsilon; \rho) = \mathbb{P} \left(\frac{|c_k^T \gamma_\star|}{\sigma \sqrt{c_k^T M_\star c_k}} > \epsilon \mid y, \rho \right), \quad (8)$$

where $c_k \in \mathbb{R}^{n+p}$ is a contrast on $\gamma_\star = (\beta^T, \gamma^T)^T$. If $c_k^T \gamma_\star = a_k^T \gamma$ for some $a_k \in \mathbb{R}^n$, then $h_k(\epsilon; \rho) = \mathbb{P} \left(\frac{|a_k^T \phi|}{\sqrt{a_k^T \text{Var}(\phi \mid y, \sigma^2, \rho) a_k}} > \epsilon \mid y, \rho \right)$ where $\text{Var}(\phi \mid y, \sigma^2, \rho)$ is given by (4).

In the context of detecting spatial disparities, consider K pairs of neighboring regions $L = \{(i, j) : i < j, i \sim j\}$, where $i \sim j$ means that regions i and j are neighbors. If $c_{ij} \in \mathbb{R}^{n+p}$ and $a_{ij} \in \mathbb{R}^n$ such that $c_{ij}^T \gamma_\star = a_{ij}^T \gamma = \gamma_i - \gamma_j$, then the corresponding ϵ -difference probability is

$$h_{ij}(\epsilon; \rho) = \mathbb{P} \left(\frac{|\phi_i - \phi_j|}{\sqrt{a_{ij}^T \text{Var}(\phi \mid y, \sigma^2, \rho) a_{ij}}} > \epsilon \mid y, \rho \right).$$

Using (1) and (2), we extend the insights obtained from Theorem 1 and show that the rankings of conditional posterior probabilities $h_1(\epsilon), \dots, h_K(\epsilon)$ are stable with respect to ϵ for any $\rho \in (0, 1)$.

Theorem 2. Let $c_1, \dots, c_K \in \mathbb{R}^{n+p}$, $X \in \mathbb{R}^{n \times p}$, and $y \in \mathbb{R}^n$ be known, and consider the model in (1) with prior $\pi(\gamma, \beta, \sigma^2) = N_n(\gamma | 0, \sigma^2 \rho V_\phi) \times N_p(\beta | M_0 m_0, \sigma^2 M_0) \times IG(\sigma^2 | a_{\sigma^2}, b_{\sigma^2})$. Define $h_k(\epsilon; \rho) = \mathbb{P} \left(\frac{|c_k^\top \gamma_\star|}{\sigma \sqrt{c_k^\top M_\star c_k}} > \epsilon \mid y, \rho \right)$ for $k = 1, \dots, K$, where $\epsilon > 0$ and $\rho \in (0, 1)$. If there exists $\epsilon_\star > 0$ such that $h_k(\epsilon_\star; \rho) < h_{k'}(\epsilon_\star; \rho)$ for any $k \neq k'$, then $h_k(\epsilon; \rho) < h_{k'}(\epsilon; \rho)$.

Proof. See Proof of Theorem 2.

If ρ has prior distribution $\pi(\rho)$, then the marginal posterior distribution of γ_\star is analytically inaccessible and we define the ϵ -difference probability for any $c_k \in \mathbb{R}^{(n+p) \times 1}$ as

$$v_k(\epsilon) = \mathbb{P} \left(\frac{|c_k^\top \gamma_\star|}{\sigma \sqrt{c_k^\top (X_\star^\top V_{y_\star}^{-1} X_\star)^{-1} c_k}} > \epsilon \mid y \right) = \int_0^1 h_k(\epsilon; \rho) \pi(\rho | y) d\rho. \quad (9)$$

Given posterior samples $\gamma_\star^{(1)}, \dots, \gamma_\star^{(N)}$ and $\rho^{(1)}, \dots, \rho^{(N)}$, we estimate (9) by

$$\widehat{v}_k(\epsilon) = \frac{1}{N} \sum_{t=1}^N \mathbb{I} \left(\frac{|c_k^\top \gamma_\star^{(t)}|}{\sigma^{(t)} \sqrt{c_k^\top \left(X_\star^\top \left(V_{y_\star}^{(t)} \right)^{-1} X_\star \right)^{-1} c_k}} > \epsilon \right), \quad (10)$$

where $V_{y_\star}^{(t)} = \begin{bmatrix} (1 - \rho^{(t)})I_n & 0 & 0 \\ 0 & M_0 & 0 \\ 0 & 0 & \rho^{(t)}V_\phi \end{bmatrix}$. Since $V_{y_\star}^{(t)}$ depends on the sampled value of $\rho^{(t)}$,

computing $\text{Var}(\gamma_\star | y, \sigma^2, \rho)$ for each posterior sample requires inverting an $(n + p) \times (n + p)$ matrix for each posterior sample, which may grow cumbersome. When we are only interested in linear combinations of the spatial effects γ , computation of $\text{Var}(\phi | y, \sigma^2, \rho)$ is sped up significantly by simultaneous reduction and a flat prior on β . Note that $\text{Var}(\phi | y, \sigma^2, \rho) = U \left(I_n + \frac{\rho}{1-\rho} D \right)^{-1} U^\top$, where U is defined in Section 2.2, is an alternate expression for (5) used in Algorithm 1.

The choice of $\pi(\rho)$ is crucial for efficiently sampling from the joint posterior of $\{\beta, \gamma, \sigma^2, \rho\}$ using MCMC and computing (10). Non-informative priors, such as a uniform distributions on $[0, 1]$, induce extreme posterior over-fitting in overly parameterized models (Gelman, 2006; Simpson et al., 2017). Instead, we consider the class of penalized complexity (PC) priors introduced in Simpson et al. (2017) as a means to encourage model parsimony and construct priors imparting better interpretation. We follow Riebler et al. (2016) by placing a PC prior on ρ , denoted by $PC(\rho; \lambda, V_\phi) \propto \lambda \exp(-\lambda d(\rho; V_\phi))$ for $0 \leq \rho \leq 1$, where $\lambda > 0$ is a fixed hyperparameter, $d(\rho; V_\phi) = \sqrt{2D_{KL}(p(y; \rho) || q(y))}$ and $D_{KL}(p(y; \rho) || q(y))$ is the Kullback-Leiber Divergence between $p(y; \rho) = N_n(y | 0_n, \rho V_\phi + (1 - \rho)I_n)$ to the base model with no structured variance $q(y) = N_n(y_{OLS} | 0_n, I_n)$. The hyperparameter λ is chosen such that $P(\rho \leq U) = a$ where U and a are constants. Riebler et al. (2016) presents promising simulation results demonstrating the PC prior's ability to shrink towards the simpler models with only spatial or non-spatial error variance.

When $\pi(\beta, \gamma, \sigma^2, \rho) = N_n(\gamma | 0, \sigma^2 \rho V_\phi) \times \text{IG}(\sigma^2 | a_{\sigma^2}, b_{\sigma^2}) \times PC(\rho | \lambda_\rho, V_\phi)$, Algorithm 2 provides Gibbs update steps for $\{\beta, \gamma, \sigma^2\}$ and a Metropolis-Hastings update step for ρ . Here, `chol` returns the upper triangular Cholesky factor of a positive definite matrix, `updateBeta` and `updateGamma` return β and γ from $\beta | y, \gamma, \sigma^2, \rho \sim N_p((F_\beta f_\beta, \sigma^2 F_\beta)$, where $F_\beta^{-1} = X^T X / (1 - \rho)$ and $f_\beta = X^T(y - \gamma) / (1 - \rho)$ and $\gamma | y, \beta, \sigma^2, \rho \sim N_n(F_\gamma f_\gamma, \sigma^2 F_\gamma)$, where $F_\gamma^{-1} = \frac{1}{1 - \rho} I_n + \frac{1}{\rho} V_\phi^{-1}$ and $f_\gamma = (y - X\beta) / (1 - \rho)$, respectively, and `updateSigmaSq` samples $\sigma^2 | y, \beta, \gamma, \rho \sim \text{InvGamma}(a_{\sigma^2} + \frac{n}{2}, b_{\sigma^2} + \frac{\|y - X\beta - \gamma\|^2}{2(1 - \rho)})$. `MHupdateRho` updates ρ using a Metropolis-Hastings random walk by proposing $1 - \rho_\star \sim \text{TruncInvGamma}(\frac{n}{2}, \frac{\|y - X\beta - \gamma\|^2}{2\sigma^2}, [0, 1])$, where we denote $Z_1 \sim \text{TruncInvGamma}(a, b, [c_L, c_U])$, $a > 0, b > 0, 0 \leq c_L < c_U$ if $\mathbb{P}(Z_1 \leq z) = \mathbb{P}(Z_2 \leq z | c_L \leq Z_2 \leq c_U)$ with $Z_2 \sim \text{IG}(a, b)$. This considerably simplifies the calculations for the acceptance probabilities in the Metropolis updates.

Algorithm 1 in Section S1 invokes updating steps in Algorithm 2 to draw posterior samples of $\{\beta, \gamma, \sigma^2, \rho\}$ in a Gibbs sampling scheme with Metropolis random walk and obtains samples of $\phi = \frac{\gamma}{\sigma\sqrt{\rho}}$. For estimating difference boundaries, Algorithm 1 takes in $c_1, \dots, c_K \in \mathbb{R}^n$ corresponding to boundaries of interest. Simultaneous reduction at the start of Algorithm 1 increases computational efficiency and facilitates Monte Carlo estimation for ϵ -difference probabilities in (10). We compute $\Delta_k = \frac{c_k^T \phi}{\sqrt{c_k^T \text{Var}(\phi | y, \sigma^2, \rho) c_k}}$ for each posterior sample of $\{\phi, \rho\}$ and $k = 1, \dots, K$. We assess predictive fit using data replicates. We draw one instance of $y_{rep}^{(t)} \sim N_n(X\beta^{(t)} + \gamma^{(t)}, \sigma^{2(t)}(1 - \rho^{(t)})I_n)$ for each drawn value of posterior samples $\{\beta^{(t)}, \gamma^{(t)}, \sigma^{2(t)}, \rho^{(t)}\}$.

3.3. Difference Probabilities in Generalized Linear Mixed Models. Stability of rankings of conditional posterior probabilities is established in the previous sections using a normally distributed outcome. More generally, for generalized linear mixed models theoretical tractability is lost when the outcome follows a probability distribution from the exponential family with link function

$$g(\mathbb{E}(y_i | \beta, \gamma_i, \eta_i)) = x_i^T \beta + \gamma_i + \eta_i, \quad (11)$$

where x_i is $p \times 1$ consisting of values of covariates for the i -th observation, $i = 1, \dots, n$, $\gamma \sim N_n(\gamma | 0_n, \sigma^2 \rho V_\phi)$, and $\eta \sim N_n(0, \sigma^2(1 - \rho)I_n)$. The link function $g(\cdot)$ relates the mean outcome to the covariates and random effects and is commonly chosen as the canonical link such that (11) is the natural parameter of the exponential family distribution of y_i .

Let $\pi(\beta, \gamma, \eta, \sigma^2, \rho) = N_p(\beta | M_0 m_0, M_0) \times N_n(\gamma | 0_n, \sigma^2 \rho V_\phi) \times N_n(\eta | 0_n, \sigma^2(1 - \rho)I_n) \times \text{IG}(\sigma^2 | a_{\sigma^2}, b_{\sigma^2}) \times \text{Beta}(\rho | a_\rho, b_\rho)$. This prior is not conditionally conjugate for non-Gaussian outcomes. Variational inference (Blei et al., 2017; Ren et al., 2011) helps in generalizing our analysis framework and provides an analytically tractable approximation to the joint posterior. We consider the hierarchical approximation $q(\gamma_\star, \eta, \sigma^2, \rho) = q(\gamma_\star | \sigma^2, \rho)q(\eta | \sigma^2, \rho)q(\sigma^2 | \rho)q(\rho)$

that approximates the conditional posterior with a Gaussian likelihood update of the form

$$q(\gamma_\star | \sigma^2, \rho) \propto \pi(\gamma_\star | \sigma^2, \rho) \times \exp\left(-\frac{1}{2\sigma^2(1-\rho)}(\gamma_\star^\top V_q \gamma_\star - 2\gamma_\star^\top m_q)\right), \quad (12)$$

where $m_q \in \mathbb{R}^{n+p}$ and $V_q \in \mathbb{R}^{(n+p) \times (n+p)}$ are fixed variational parameters. The approximate conditional posterior is $q(\gamma_\star | \sigma^2, \rho) = N_{n+p}(M_\star m_\star, \sigma^2 M_\star)$, where $M_\star^{-1} = \frac{1}{1-\rho}V_q + \frac{1}{\rho}W_\phi^{-1}$, $m_\star = V_q m$, and $W_\phi^{-1} = \begin{bmatrix} 0_{p \times p} & 0_{p \times n} \\ 0_{n \times p} & V_\phi^{-1} \end{bmatrix}$. We choose $q(\eta | \sigma^2, \rho) = N_n(m_\eta, V_\eta)$ with variational parameters $m_\eta \in \mathbb{R}^n$ and $V_\eta \in \mathbb{R}^{n \times n}$, which assumes η and γ_\star are independent given (σ^2, ρ) in the approximation since η captures non-structured error. To ensure the $q(\gamma_\star, \eta, \sigma^2, \rho)$ is proper, V_q must be positive semi-definite and V_η must be positive definite.

The approximation $q(\sigma^2 | \rho)q(\rho)$ follows a similar form to the conditional posterior of (3) for Gaussian outcomes,

$$q(\sigma^2 | \rho) = \text{IG}\left(\theta_1, \theta_2 + \frac{1}{1-\rho}\theta_3 - \theta_4 m_\star^\top M_\star m_\star\right), \quad q(\rho) = \text{Beta}(\theta_5, \theta_6) \quad (13)$$

where $\theta_1 > 0$, θ_2 , θ_3 , and θ_4 are the fixed variational parameters. Here, $\theta_2 + \frac{1}{1-\rho}\theta_3 - \theta_4 m_\star^\top M_\star m_\star > 0$ must hold for all $\rho \in (0, 1)$. Finally, the Beta approximation distribution for $q(\rho)$ is a natural choice in the exponential family since ρ is constrained to lie in $(0, 1)$.

For (1), the approximation distribution reduces to $q(\gamma_\star, \sigma^2, \rho) = q(\gamma_\star | \sigma^2, \rho)q(\sigma^2 | \rho)q(\rho)$. The conditional posterior $\pi(\gamma_\star, \sigma^2 | y, \rho)$ in (3) can be recovered exactly through the approximation $q(\gamma_\star, \sigma^2 | \sigma^2, \rho)q(\sigma^2 | \rho)$ by setting $m_q = (y^\top X, y^\top)^\top$, $V_q = (X^\top, I_n)(X^\top, I_n)^\top$, $\theta_1 = a_n$, $\theta_2 = b_{\sigma^2} + \frac{1}{2}m_0^\top M_0 m_0$, $\theta_3 = \frac{1}{2}y^\top y$, and $\theta_4 = \frac{1}{2}$ in (12) and (13). In general, the approximation parameters, m_q , V_q , m_η , V_η , and $\theta = (\theta_1, \dots, \theta_6)$, are chosen to minimize the Kullback-Leiber divergence between $q(\beta, \gamma, \eta, \sigma^2, \rho)$ and $\pi(\beta, \gamma, \eta, \sigma^2, \rho | y)$. Since all conditional approximation distributions are members of the exponential family, the numerical optimization problem of minimizing the Kullback-Leiber divergence can be efficiently solved by, for example, the stochastic optimization algorithm proposed by [Salimans and Knowles \(2013\)](#).

Difference probabilities are then defined with respect to the posterior approximation as $v_k(\epsilon) = \mathbb{P}_q\left(\frac{|c_k^\top \gamma_\star|}{\sqrt{\text{Var}_q(c_k^\top \gamma_\star | y, \sigma^2, \rho)}} > \epsilon \mid y\right)$, where $\text{Var}_q(c_k^\top \gamma_\star | y, \sigma^2, \rho) = \sigma^2 \sqrt{c_k^\top M_\star c_k}$. Since the approximate conditional posterior of (γ_\star, σ^2) is a normal-inverse-gamma distribution, the conditional difference probability in (8) defined with respect to q is rank-stable for a fixed ρ (Proof of Theorem 2). This extends the result of Theorem 2 to any generalized linear mixed model under the variational approximation.

The variational approximation comes with a cost. First, variational inference generally underestimates the posterior variance due to the nature of the Kullback-Leibler divergence minimization (see, e.g., [Blei et al., 2017](#); [Ren et al., 2011](#)). Furthermore, the Gaussian approximation may not always be appropriate for every likelihood function. We refer to [Fischer et al. \(2025\)](#) for theory on

approximation quality of a Gaussian distribution for the posterior in exponential families. Instead of the variational approximation, we could use samples from the exact posterior obtained via MCMC methods to estimate difference probabilities of the form

$$\tau_k(\epsilon) = \mathbb{P} \left(\frac{|c_k^\top \beta_\star|}{\sqrt{\text{Var}(c_k^\top \beta_\star | y)}} > \epsilon \mid y \right), \quad (14)$$

where $\beta_\star = (\beta^\top, \phi^\top)^\top$. Let $\bar{\beta}_\star = \frac{1}{T} \sum_{t=1}^T \beta_\star^{(t)}$, then the marginal posterior variance is estimated as $\widehat{\text{Var}}_q(c_k^\top \beta_\star | y) = \frac{1}{T-1} \sum_{t=1}^T (c_k^\top \beta_\star - c_k^\top \bar{\beta}_\star)^2$. The rankings of the difference probabilities may still be stable without a variational approximation if the marginal posterior distribution of β_\star resembles, for example, a multivariate normal or t-distribution.

We remark that both approaches share a weakness for detecting spatial disparities: the choice of the link function $g(x)$ in (11) critically determines the scale of spatial effects in high-risk versus low-risk regions. For example, if $g(x) = \log(x)$, the canonical link for a Poisson generalized linear model, then $\mathbb{E}[y_i | \beta, \gamma_i = 1, \eta_i] = \exp(1) \cdot \mathbb{E}[y_i | \beta, \gamma_i = 0, \eta_i]$, indicating that the magnitude of the spatial effect γ_i depends implicitly on the magnitude of $x_i^\top \beta$. Hence, difference probabilities corresponding to boundaries in high-risk boundaries may be ranked lower than those in low-risk regions with equivalent geographic heterogeneity in observed rates; we demonstrate this through a simulation example in Section 4.3 with the difference probability defined in (14). We otherwise focus our attention on the case of a normally distributed outcome and identity link function, applying equal weight to differences between rates in high-risk and low-risk regions.

3.4. A Bayesian FDR-Based Decision Rule. After computing the difference probability $v_k(\epsilon)$ for each linear combination of interest, we wish to account for multiple comparisons before constructing binary decisions because we are not operating under an automatically penalizing mixture model as in [Scott and Berger \(2006\)](#). We specifically consider safeguarding against Type I errors by controlling the false discovery rate (FDR introduced in [Benjamini and Hochberg, 1995](#)), while retaining

power by minimizing the false negative rate (FNR). Thus, we define $\text{FDR} = \frac{\sum_{k=1}^K \mathbb{I} \left(\frac{|c_k^\top \gamma_\star|}{\sigma \sqrt{c_k^\top M_\star c_k}} \leq \epsilon \right) d_k}{c + \sum_{k=1}^K d_k}$,

$\text{FNR} = \frac{\sum_{k=1}^K \mathbb{I} \left(\frac{|c_k^\top \gamma_\star|}{\sigma \sqrt{c_k^\top M_\star c_k}} > \epsilon \right) (1-d_k)}{c + \sum_{k=1}^K (1-d_k)}$ where $c > 0$ is a small constant to avoid a zero denominator and

$d_k \in \{0, 1\}$ represents our decision to declare $\frac{|c_k^\top \gamma_\star|}{\sigma \sqrt{c_k^\top M_\star c_k}} > \epsilon$. As explained in [Müller et al. \(2007\)](#), the FDR and FNR functions are random variables that have distinct interpretations in the two paradigms.

Given a set of difference probabilities $\{v_1(\epsilon), \dots, v_K(\epsilon)\}$, we use the Bayesian FDR and FNR defined in Müller et al. (2004) as the posterior expectation

$$\overline{\text{FDR}}(t^*, \epsilon) = \mathbb{E}[\text{FDR}(t^*, \epsilon) | y] = \frac{\sum_{k=1}^K (1 - v_k(\epsilon)) \mathbf{I}(v_k(\epsilon) \geq t^*)}{\sum_{k=1}^K \mathbf{I}(v_k(\epsilon) \geq t^*)}, \quad (15)$$

$$\overline{\text{FNR}}(t^*, \epsilon) = \mathbb{E}[\text{FNR}(t^*, \epsilon) | y] = \frac{\sum_{k=1}^K v_k(\epsilon) \mathbf{I}(v_k(\epsilon) < t^*)}{\sum_{k=1}^K \mathbf{I}(v_k(\epsilon) < t^*)}. \quad (16)$$

Minimizing the $\overline{\text{FNR}}$ subject to $\overline{\text{FDR}} \leq \delta$ is achieved by decisions of the form $d_k = \mathbf{I}(v_k(\epsilon) \geq t^*(\epsilon))$, where $t^*(\epsilon) \in [0, 1]$ for all $\epsilon > 0$ is a threshold chosen as

$$t^*(\epsilon) = \inf \left\{ t \in [0, 1] : \overline{\text{FDR}}(t, \epsilon) \leq \delta \right\}. \quad (17)$$

Bayesian and classical FDR compute posterior probabilities and p-values, respectively, which are used to rank the plausibility of each hypothesis before choosing a cutoff according to a decision rule. In general, the Bayesian FDR and its classical analogue are fundamentally different criterion that are not necessarily equivalent and their respective control procedures may produce different sets of decisions. However, in the linear fixed effects model and the setting of Theorem 1, if the prior is non-informative on β in the Bayesian approach, then the order of the posterior probabilities is the reversed order of the p-values. In this case, the Bayesian and classical FDR control procedures differ only in the decision criterion; specific choice of the decision parameter δ in the Bayesian approach can afford decisions identical to many classical FDR control procedures.

For creating binary decisions, ϵ must be chosen to apply this Bayesian FDR control procedure. However, for any $\delta > 0$, if we set ϵ to be arbitrarily small and $t^* = 0$, we would declare every decision positive as $d_k = 1$. On the other hand, if we set ϵ to be arbitrarily large and $t^* = 1$, then we would declare every decision negative as $d_k = 0$. Both cases achieve $\overline{\text{FDR}} \leq \delta$ but do not induce meaningful statements about the data. This motivates a heuristic to choose ϵ at a reasonable value before applying the Bayesian FDR control procedure to create decisions.

3.5. Selecting an ϵ -difference threshold. In the absence of guidance on the choice of ϵ , we consider two general heuristics to select a reasonable value for ϵ , the first based on a loss function and the relation between ϵ and our resulting actions. As ϵ increases, the event $\frac{|c_k^T \gamma_\star|}{\sigma \sqrt{c_k^T M_\star c_k}} > \epsilon$ gains stronger meaning, but has a lower posterior probability. On the other hand, the event $\frac{|c_k^T \gamma_\star|}{\sigma \sqrt{c_k^T M_\star c_k}} \leq \epsilon$ becomes less precise but more probable. This motivates the use of a loss function that is optimized with respect to ϵ by balancing the strength of our affirmative conclusions that $\frac{|c_k^T \gamma_\star|}{\sigma \sqrt{c_k^T M_\star c_k}} > \epsilon$ with the precision of our negative conclusions that state $\frac{|c_k^T \gamma_\star|}{\sigma \sqrt{c_k^T M_\star c_k}} \leq \epsilon$.

As a general heuristic, we appeal to the principle of maximum entropy, which suggests that, given a selection of possible posterior distributions, the posterior distribution that best represents our posterior knowledge is precisely the one with maximum entropy. The principle of maximum

entropy (Jaynes, 1957) selects the maximum entropy distribution due to it being “maximally noncommittal” with respect to the amount of information we imbue the posterior with beyond the observed data. Under the model (1), choosing an extremely small or large difference threshold ϵ causes the posterior distribution of $r_k(\epsilon) = \mathbb{I}\left(\frac{|c_k^T \gamma_\star|}{\sigma \sqrt{c_k^T M_\star c_k}} > \epsilon\right)$ to collapse into a point mass at 1 or 0 respectively, which has minimal entropy. Maximizing the joint posterior entropy of $R = \{r_1(\epsilon), \dots, r_K(\epsilon)\}$ with respect to ϵ thus avoids obscuring the information that the data y provides on the true quantities of interest, $\left\{\frac{|c_1^T \gamma_\star|}{\sigma \sqrt{c_1^T M_\star c_1}}, \dots, \frac{|c_K^T \gamma_\star|}{\sigma \sqrt{c_K^T M_\star c_K}}\right\}$.

Shannon (1948) explains the Shannon entropy as an objective measure of the information or uncertainty of a probability distribution. Let I be a $K \times 1$ vector such that $I_k \in \{0, 1\}$ for all $k = 1, \dots, K$ and let $g(I) = \mathbb{P}(\cap_{k=1}^K r_k(\epsilon) = I_k | y)$. Since $r_k(\epsilon)$ is a binary random variable equal to 1 with posterior probability $v_k(\epsilon)$, the joint Shannon posterior entropy of R measured in nats is defined as $H(R) = -\sum_{I \in \{0,1\}^K} g(I) \log g(I)$. However, the joint entropy entails estimating 2^K probabilities and is computationally unfeasible even for moderate K .

Instead, we opt for maximizing the entropy of a uniformly chosen ϵ -difference indicator. For any $\epsilon > 0$, let J be a random variable with uniform probability mass on $\{1, \dots, K\}$ and $W = r_J(\epsilon)$. The conditional posterior entropy of W given J is $H_J(W) = \sum_{k=1}^K H(r_k(\epsilon)) P(J = k) = \frac{1}{K} \sum_{k=1}^K H(r_k(\epsilon))$. The sum of the individual entropies is related to the joint entropy by the sub-additivity property of the joint entropy (Shannon, 1948), which states that $H(R) \leq \sum_{k=1}^K H(r_k(\epsilon)) = -\sum_{k=1}^K v_k(\epsilon) \log v_k(\epsilon) + (1 - v_k(\epsilon)) \log(1 - v_k(\epsilon))$. We obtain an optimal ϵ by maximizing the average of the individual entropies or, equivalently, minimizing

$$\text{LOSS}_{\text{CE}}(\epsilon) = \sum_{k=1}^K v_k(\epsilon) \log v_k(\epsilon) + (1 - v_k(\epsilon)) \log(1 - v_k(\epsilon)), \quad (18)$$

which we refer to as the conditional entropy loss function. We denote the ϵ obtained from minimising (18) as ϵ_{CE} . When $v_k(\epsilon)$ is unavailable in closed form, this loss function is estimated from the posterior samples using (7). For difference boundary analysis on a set L containing K pairs of neighboring regions and a corresponding set of difference probabilities, $\{v_{ij}(\epsilon)\}_{(i,j) \in L}$, the summation in (18) is over all pairs of neighboring regions, $(i, j) \in L$. Also, $v_k(\epsilon)$ is replaced with $h_k(\epsilon; \rho)$ defined in (8) when conditioning on a given $0 < \rho < 1$.

As an alternative to optimizing (18), we can consider the number of positive decisions denoted by T . Fixing two quantities out of ϵ , δ and T determines the third, representing a three-way trade-off between protection against Type I errors, quantity, and quality in our positive results: δ indicates our tolerance for false positives; T is the quantity of positive results; and ϵ is our standard for a disparity, which reflects the quality of our decisions. If the maximum allowable Bayesian FDR, δ , and the number of decisions, T , are fixed, then a valid choice of ϵ should belong to $A_\epsilon = \left\{\epsilon > 0 : \overline{\text{FDR}}(t^\star(\epsilon)) \leq \delta, |S(\epsilon)| \geq T\right\}$. This criterion can be more useful in policy settings aiming to identify rankings of the most egregious disparities, for example, the top fifty. Finally,

by fixing ϵ and T , δ implicitly equals the Bayesian FDR of the resulting decisions, although this represents no active protection against Type I errors.

We conclude this section with a remark regarding the implications of the limiting cases discussed in Section 2.2. As ρ tends to 0, boundary detection becomes meaningless because the spatial effects converge to 0. As ρ tends to 1, σ^2 and γ also have limiting distributions described at the end of Section 2.2. These results suggest that the conditional variance of γ (in the definition of the ϵ -difference probability) or σ^2 will neither explode nor shrink toward 0 when ρ is near 1.

4. SIMULATION EXPERIMENTS

4.1. Exact Conjugate BYM2 Model. To assess our proposed framework for detecting spatial disparities, we conduct a simulation experiment by generating data over 3,078 contiguous U.S. counties. We first investigate an exact sampling scheme that conditions on a fixed value of ρ and places a conditionally autoregressive (CAR) structure on the precision matrix of the spatial random effects. We use (1) and construct $V_\phi^{-1} = c(D_W - \alpha W)$ with W encoding the neighbors of U.S. counties. We generate the spatial random effects ϕ using $\alpha = 0.99$, scaling factor $c = 0.365$ and covariates $X = (1_n, x)$, where $x \sim N_n(0, I_n)$ and simulate the observed data y using (1) with $\sigma^2 = 4$, $\rho = 0.93$, and $\beta = (2, 5)^T$.

We investigate spatial difference boundary detection on the set of all pairs of neighboring counties, $L = \{(i, j) : i < j, i \sim j\}$. The indicator of a true spatial disparity for pair (i, j) and a given difference threshold ϵ is defined as $r_{ij}(\epsilon) = \mathbf{I}\left(\frac{|\phi_i - \phi_j|}{\sqrt{c_{ij}^T \text{Var}(\phi | y, \sigma^2, \rho) c_{ij}}} > \epsilon\right)$, evaluated using the true values of ϕ and ρ . For the simulated data, there are $K = 9,119$ distinct pairs of adjacent counties. Using the prior $\pi(\gamma, \beta, \sigma^2) = N(\gamma | 0, \sigma^2 \rho V_\phi) \times N(\beta | M_0 m_0, \sigma^2 M_0) \times \text{IG}(\sigma^2 | a_{\sigma^2}, b_{\sigma^2})$ with $M_0^{-1} = 10^{-4} I_2$, $m_0 = 0_p$, $a_{\sigma^2} = 0.1$, and $b_{\sigma^2} = 0.1$, we generate 10,000 exact samples from the posterior distribution of ϕ extracted from γ in (3). Figure S2 in Section S3 compares posterior predictive means with observed values and reveals an excellent fit.

Given $\rho = 0.93$, we use posterior samples of $(\beta, \gamma, \sigma^2)$ to compute Monte Carlo estimates of $\{h_{ij}(\epsilon)\}_{(i,j) \in L}$ defined in (8), which we treat as the difference probabilities in the conditional entropy loss in (18). By numerically minimizing the conditional entropy loss, we obtain the optimal threshold as $\epsilon_{CE} = 1.296$. Figure 1 displays the loss function evaluated at ϵ and a histogram of $\{h_{ij}(\epsilon_{CE})\}_{(i,j) \in L}$, showing a cluster of probabilities near 1 that correspond to strong posterior evidence of a spatial disparity using $\epsilon_{CE} = 1.296$ as the difference threshold.

With $\epsilon_{CE} = 1.296$, we use the Bayesian FDR control procedure discussed in Section 3.4 to classify boundaries as spatial disparities by considering the conditional posterior probabilities $\{h_{ij}(\epsilon_{CE})\}_{(i,j) \in L}$ as the difference probabilities. We first use the Monte Carlo estimates of $\{h_{ij}(\epsilon_{CE})\}_{(i,j) \in L}$ to estimate the Bayesian FDR and FNR as defined in (15) and (16) respectively before selecting a cutoff posterior probability t_\star according to (17) with Bayesian FDR tolerance $\delta = 0.10$, which results in setting $t_\star = 0.6479$ and declaring 4,540 boundaries as spatial disparities.

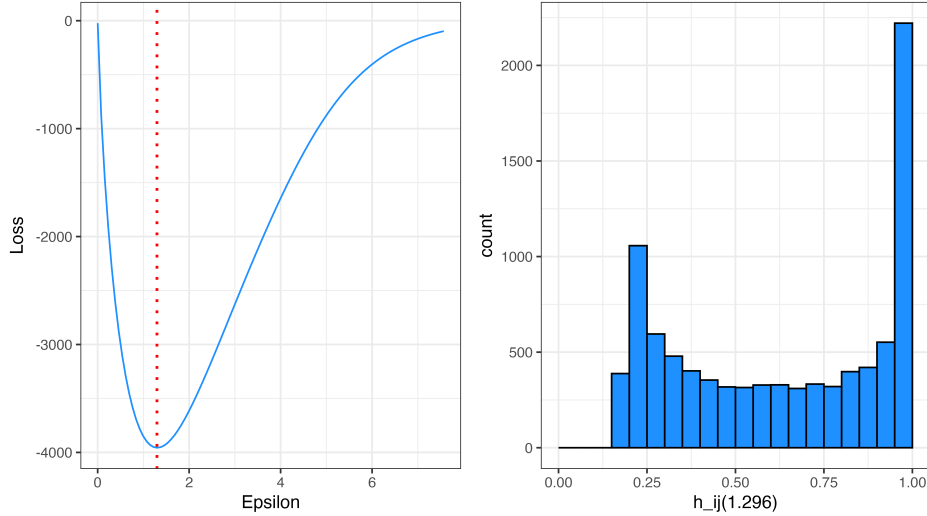


FIGURE 1. Left: conditional entropy loss function evaluated across ϵ with a dotted line indicating the numerically optimal difference threshold $\epsilon_{CE} = 1.296$. Right: histogram of the resulting posterior probabilities $\{h_{ij}(\epsilon_{CE})\}_{(i,j) \in L}$.

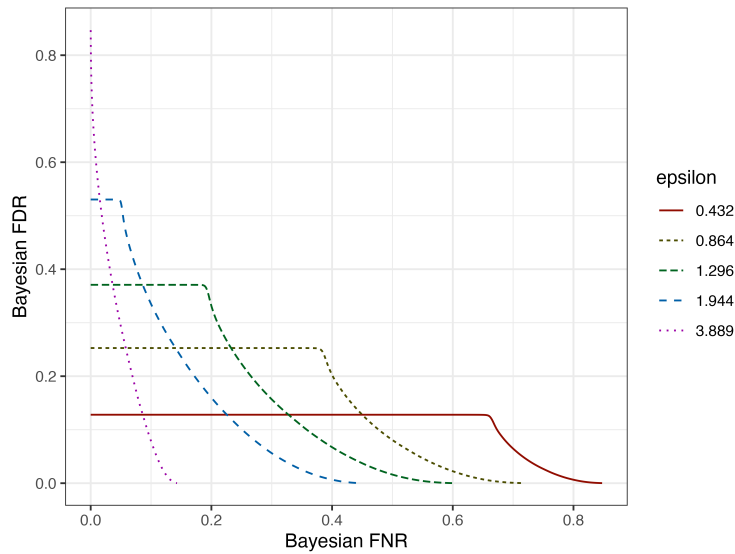


FIGURE 2. Bayesian FDR against FNR curves for different values of ϵ .

According to the true values of ϕ , 4,562 out of 9,119 boundaries are a spatial disparity with the same $\epsilon_{CE} = 1.296$ difference threshold. Comparing with true disparities, we achieve approximately 71.2% sensitivity, 86.2% specificity, 76.8% accuracy, a true false discovery rate of 10.2%, and a true false negative rate of 36.3%. As discussed in Section 3.4, the true false discovery rate exceeds $\delta = 0.1$ because δ represents tolerance for Bayesian FDR, which is a metric fundamentally different from classical FDR control procedures.

We illustrate the effect of ϵ on the Bayesian FDR and FNR by evaluating the estimated Bayesian FDR and FNR as functions of the cutoff t for multiple fixed values of ϵ . Figure 2 shows FDR versus FNR curves for $\epsilon \in \{0.432, 0.864, 1.296, 1.944, 3.889\}$. The goal for any given ϵ is to minimize the Bayesian FNR under the constraint that Bayesian FDR $\leq \delta$, but Figure 2 demonstrates that the FDR versus FNR curve becomes increasingly steep near 0. According to our posterior belief, there are few disparities at large values of ϵ , so the Bayesian FNR and FDR suggest fewer boundaries as disparities. On the other hand, decreasing ϵ causes the FDR versus FNR curve to plateau at a lower FDR value because the event that each difference exceeds the ϵ threshold becomes more probable and occurs with nearly probability one for small enough ϵ . This behavior of the Bayesian FDR and FNR motivates the criteria in Section 3.5 for selecting a reasonable value of ϵ before accounting for multiplicity by controlling the Bayesian FDR.

Since the probabilities $\{h_{ij}(\epsilon_{CE})\}_{(i,j) \in L}$ are computed conditional on exact knowledge of ρ , their rankings are theoretically stable by Theorem 2. Figure S3 displays stable rejection paths of the difference probabilities for values of ϵ surrounding the chosen threshold ϵ_{CE} , but the instability in the low ranks of the rightmost graph are due to imprecise Monte Carlo estimates of posterior probabilities near zero with a large difference threshold, $\epsilon = 3.889$. Figure S3 shows that high ranks of difference probabilities correspond to true disparities, demonstrating the efficacy of our method in the exact sampling setting.

4.2. Placing a prior on ρ . In practice, the true value of ρ , the approximate proportion of variance attributable to the spatial CAR structure, is not known. The choice of ρ to condition on can be regarded as a model selection problem, where common approaches are based on information criteria, such as the DIC as introduced in Spiegelhalter et al. (2002) and the WAIC, introduced by Watanabe (2010). The DIC and WAIC values are computed using the predictive distribution $Y | \beta, \gamma, \sigma^2, \rho \sim N_n(X\beta + \gamma, \sigma^2(1-\rho)I_n)$ and penalize complexity, such as p_{DIC} and p_{WAIC2} (Gelman et al., 2014). However, for the model given by (1) and conditioned on a given $\rho \in (0, 1)$, each metric decreases asymptotically to $-\infty$ as $\rho \rightarrow 1^-$, regardless of the true value of ρ used to generate the data. This is supported both by simulation and analytical arguments in Sections S4 and S5. Gelman et al. (2014) explains that WAIC and DIC estimate the out-of-sample prediction error, which is nearly erased when $\rho \approx 1$ indicates a spatially dominant model with negligible measurement error. Intuitively, the DIC and WAIC metrics cannot account for over-fitting as $\rho \rightarrow 1^-$ and $\|y - X\beta - \gamma\|^2$ converges in probability to 0. Hence, we cannot apply model selection based on the specified predictive distribution to obtain a value of ρ to condition on.

We pivot to posterior inference with a prior on ρ . We use the simulated data in Section 4.1. We specify the joint prior as $\pi(\beta, \gamma, \sigma^2, \rho) \propto N_n(\gamma | 0, \sigma^2 \rho V_\phi) \times \text{IG}(\sigma^2 | a_{\sigma^2}, b_{\sigma^2}) \times \text{PC}(\rho | \lambda_\rho)$, where $a_{\sigma^2} = 0.1$ and $b_{\sigma^2} = 0.1$. For the PC prior on ρ , we follow Riebler et al. (2016) and choose $\lambda_\rho = 0.0335$ such that $\mathbb{P}(\rho < 0.5) \approx \frac{2}{3}$. We apply Algorithm 1 to draw 30,000 posterior samples

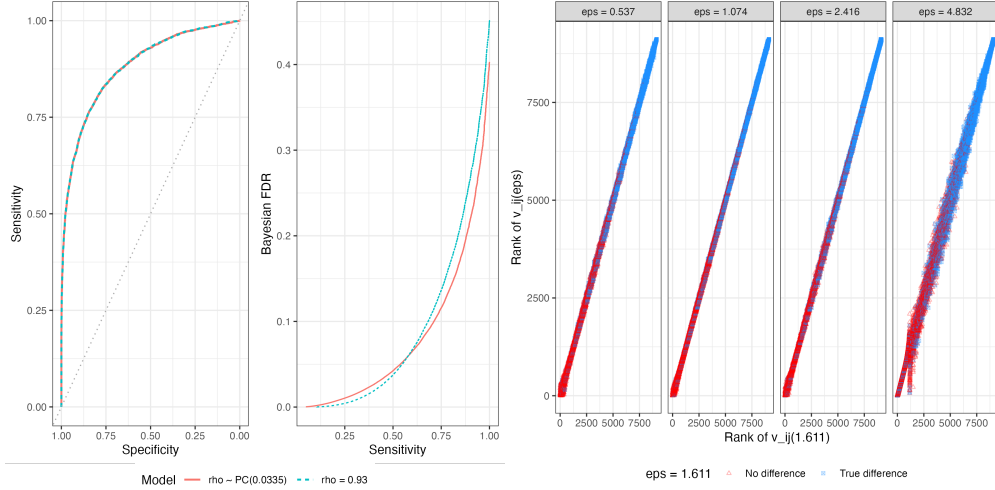


FIGURE 3. Classification performance of spatial disparity detection on simulated data when drawing exact samples conditional on $\rho = 0.93$ versus placing a PC prior on ρ and using Metropolis within Gibbs sampling and fixed difference threshold $\epsilon = 1.611$. Left: ROC curves for each model. The area under each ROC curve is 0.881. Middle: Bayesian FDR versus true sensitivity. Right: Simulated rankings of ϵ -difference probabilities $\{v_{ij}(\epsilon)\}_{(i,j) \in L}$ for $\epsilon = 0.537, 1.074, 2.417, 4.833$ versus rankings of $\{v_{ij}(\epsilon_{CE})\}_{(i,j) \in L}$ using a PC prior on ρ . Disparities according to the true values of ϕ and ρ are shown in blue.

of $(\beta, \gamma, \sigma^2, \rho)$ after discarding 10,000 initial burn-in samples. A 95% credible interval for ρ is $(0.867, 0.991)$, showing that our algorithm can effectively learn about ρ .

Since we only consider spatial effect differences across geographic boundaries, the ϵ -difference probability in (9) simplifies to $v_{ij}(\epsilon) = \mathbb{P}\left(\frac{|\phi_i - \phi_j|}{\sqrt{a_{ij}^T \text{Var}(\phi | y, \sigma^2, \rho) a_{ij}}} > \epsilon \mid y\right)$, where $(i, j) \in L$ is a pair of neighboring counties and a_{ij} is $n \times 1$ with 1 and -1 as its i th and j th element, respectively, and 0 elsewhere. We compute Monte Carlo estimates of $\{v_{ij}(\epsilon)\}_{(i,j) \in L}$ using (10) and minimize the conditional entropy loss function in (18) to obtain $\epsilon_{CE} = 1.611$ as the optimal difference threshold. We compare classification performance of placing a PC prior on ρ with that of fixing ρ (Section 4.1) by plotting ROC curves that display sensitivity and specificity for both settings. Moving on the ROC curve from left to right implicitly decreases the classification threshold or increases the Bayesian FDR tolerance δ . The left panel in Figure 3 shows nearly identical ROC curves for sampling with a fixed ρ and a PC prior on ρ , which indicates similar performance up to the classification threshold. The middle panel of Figure 3 displays the estimated Bayesian FDR versus the true sensitivity for both models and reveals negligible impact of the prior for ρ on the behavior of Bayesian FDR. Setting $\delta = 0.1$ achieves approximately 70% sensitivity and $\delta = 0.05$ achieves approximately 50% sensitivity when placing a PC prior on ρ .

We also evaluate the stability of the rankings of the ϵ -difference probabilities $\{v_{ij}(\epsilon)\}_{(i,j)\in L}$. The right panel of Figure 3 shows that the rankings are slightly shifted when the difference threshold is tripled to $\epsilon = 4.833$, but remain stable when increasing or decreasing the difference threshold ϵ_{CE} by 50%. Hence, the rejection path that our method produces in this instance is reasonably robust to selection of the difference threshold ϵ .

We remark that simulation experiments in Section S2 demonstrate that our method is able to effectively detect sharp difference boundaries and even outperforms the more computationally intensive areally-referenced Dirichlet process (ARDP) devised by Li et al. (2015) in terms of classification performance. Both methods are most effective when ρ , the proportion of spatial variance, is large relative to noise.

4.3. Simulated Count Outcome. We demonstrate our analysis framework for a count outcome simulated over a map of the $n = 58$ Californian counties. We simulate $\gamma \sim N_n(0_n, \sigma^2 \rho W_\phi)$ and $\eta \sim N_n(0_n, \sigma^2(1 - \rho)I_n)$ with $\sigma^2 = 2, \rho = 0.93$, and W_ϕ as a exponential covariance kernel such that $W_{\phi,ij} = \exp(-d_{ij}/50)$, where d_{ij} is the great circle distance between the centroids of county i and j in kilometers. We split the counties into a high-risk, low-exposure region in the north and low-risk, high-exposure region in the south. For counties with centroids whose latitude coordinate is above 37.852, we generate $x_i = (1, x_{i1})^T, x_{i1} \sim N(2, 1)$ and $E_i = [E_H], E_H \sim \text{Unif}(10^4, 5 \cdot 10^4)$. For counties with centroids whose latitude coordinate is 37.852 or lower, we draw $x_i = (1, x_{i1})^T, x_{i1} \sim N(-2, 1)$ and $E_i = [E_L], E_L \sim \text{Unif}(5 \cdot 10^4, 5 \cdot 10^5)$. For $i = 1, \dots, 58$, we simulate $y_i \sim \text{Poisson}(E_i \exp(x_i^T \beta + \gamma_i + \eta_i))$ with $\beta = (-5, 0.5)^T$. Here, we define the simulated rate as Y_i/E_i and denote the boundary between county i and j as a true spatial disparity at the ϵ -difference level if $\frac{|\phi_i - \phi_j|}{a_{ij}^T W_\phi a_{ij}} > \epsilon$.

We analyze the simulated data using a Poisson likelihood with the link function in (11) as $g(x) = \log\left(\frac{x}{E_i}\right)$ and use the prior $\pi(\beta, \gamma, \eta, \sigma^2, \rho) \propto N_n(\gamma | 0_n, \sigma^2 \rho V_\phi) \times N_n(\eta | 0_n, \sigma^2(1 - \rho)I_n) \times \text{IG}(\sigma^2 | 0.1, 0.1) \times \text{Unif}(\rho | 0, 1)$. We place a CAR spatial prior on γ by fixing $V_\phi^{-1} = c(D_W - \alpha W)$ using the adjacency relations of the Californian counties, $\alpha = 0.99$, and $c = 0.8352$. Using Hamiltonian Monte Carlo implemented within the rstan package in R, we obtain $20,000 \times 4$ chains = 80,000 total posterior samples of $(\beta, \gamma, \sigma^2, \rho)$ after discarding 40,000 initial burn-in samples per chain. We consider L , the set of boundaries between two neighboring Californian counties, and use Monte Carlo estimates of $\{\tau_{ij}(\epsilon)\}_{(i,j)\in L}$ via (14) to minimise the conditional entropy loss and obtain the optimal difference threshold $\epsilon_{CE} = 0.728$. Out of 139 total boundaries, 66 are a true disparity at the $\epsilon_{CE} = 0.728$ difference level.

The left two graphs in Figure 4.3 shows clear hotspots in the simulated rate map, but a majority of the boundaries in L_S , a subset of L corresponding to the top 40 values of $v_{ij}(\epsilon_{CE})$, are between counties with simulated rates less than 0.05 because a logarithmic link function favors reporting disparities in low-risk regions (Section 3.3). These boundaries correspond to clearer visual differences on the log-rate map. Nonetheless, we use the difference probabilities $\{v_{ij}(\epsilon)\}_{(i,j)\in L}$ to detect spatial

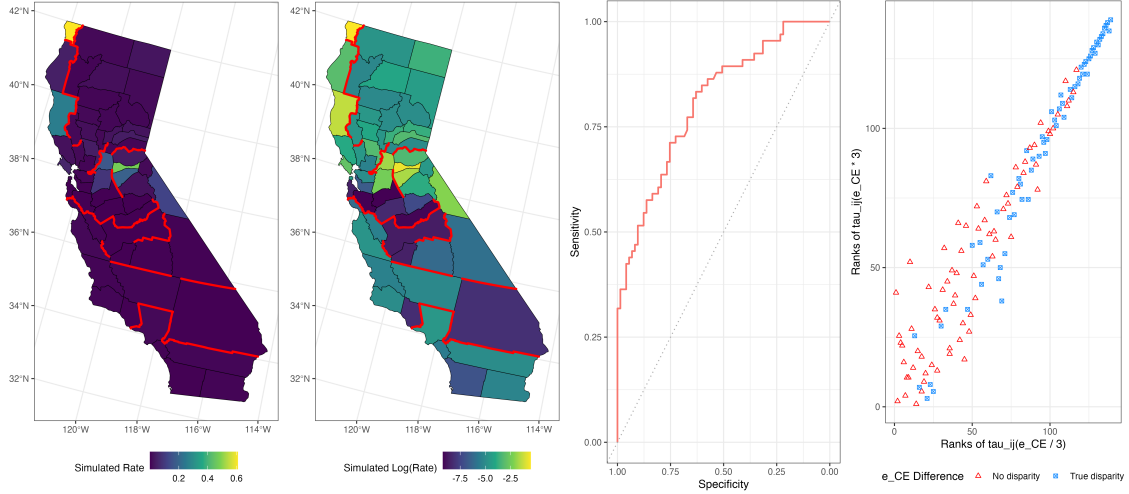


FIGURE 4. Classification results for simulated count outcome. Left: Boundaries associated with top 40 $\epsilon_{CE} = 0.728$ difference probabilities overlaid on simulated rate and log-rate map. Middle: ROC curve. The area under the curve is 0.809. Right: Ranks of $\{\tau_{ij}(3\epsilon_{CE})\}_{(i,j)\in L_S}$ versus $\{\tau_{ij}(\frac{1}{3}\epsilon_{CE})\}_{(i,j)\in L_S}$.

disparities and obtain favorable classification performance shown by the ROC curve in the middle panel of Figure 4.3. The right panel of Figure compares the ranks of $\{\tau_{ij}(\frac{1}{3}\epsilon_{CE})\}_{(i,j)\in L_S}$ against $\{\tau_{ij}(3\epsilon_{CE})\}_{(i,j)\in L_S}$. The sample Spearman rank correlation between the two sets is $r_s = 0.9726$, which we consider as a rank stability score.

We repeat the analysis with an alternative difference probability definition, $\tau_{ij} = \mathbb{P}(|\phi_i - \phi_j| > \epsilon | y)$. For a fair comparison, we also redefine a pair (i, j) to be a true spatial disparity on the ϵ -difference level if $|\phi_i - \phi_j| > \epsilon$. The resulting AUC is 0.7684 and rank stability score is 0.8411, indicating that our proposed difference probability formulation improves classification performance and adds robustness to the rankings of the top difference probabilities in this simulation example.

5. APPLICATION

We analyze publicly available health data from the Institute of Health Metrics and Evaluation (IHME) on age-standardized US county-level estimates of mortality rates across tracheal, bronchus, and lung cancer in 2014 (Mokdad et al., 2017). We incorporate one predictor, county-level estimates of total (non-daily and daily) smoking prevalence in both sexes in 2012 originally derived using data from the Behavioral Risk Factor Surveillance System in Dwyer-Lindgren et al. (2014). Previous work by (Shreves et al., 2023) indicates that lung cancer mortality rates exhibit spatial autocorrelation that is not completely accounted for by smoking prevalence.

For our study region, we subset to $n = 3,017$ contiguous U.S. counties with available estimates for smoking prevalence and lung cancer mortality rates with the intent of detecting disparities corresponding to county boundaries. While we drop counties with missing data for the sake

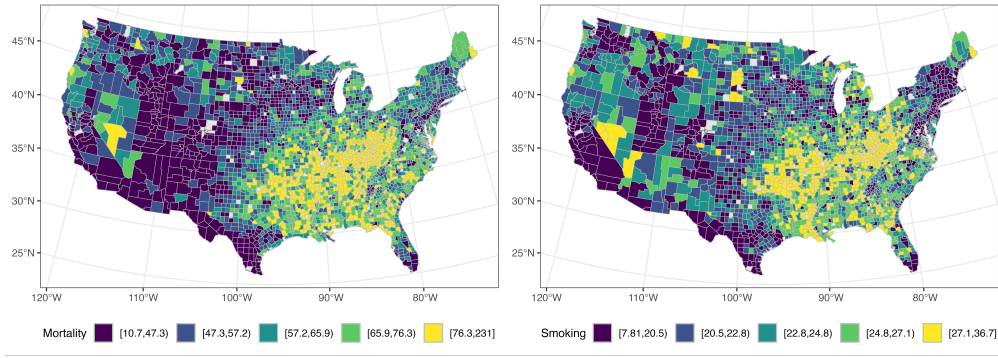


FIGURE 5. Left: map of county-level age-standardized mortality rate estimates for lung cancer in 2014, colored by quintile. Right: map of county-level total smoking prevalence estimates in 2012, colored by quintile.

of simplicity in this application, one can refer to [Rubin \(1976\)](#) for an introduction to Bayesian approaches to missing data or [Ma and Chen \(2018\)](#) for a modern overview. For simplicity, we drop these counties from our study region as the remaining counties form a contiguous region. The cancer mortality rate and total smoking prevalence estimates of the final study region are mapped in Figure 5. High risk regions can clearly be identified most notably in the East South Central states and our analysis aims to identify local health inequity on the county-level.

To assess spatial autocorrelation, we fit an ordinary least squares linear model with an intercept and smoking prevalence as a predictor of lung cancer mortality before computing Moran’s $I = 0.4563$ and Geary’s $C = 0.5330$ using the residuals ([Banerjee et al., 2015](#)). Both statistics were significant under 10,000 random permutations (p-value = $1/10,001$) suggesting that spatial autocorrelation is not fully captured by linearly regressing mortality rates on smoking prevalence.

We employ (1) such that $y | \beta, \gamma, \sigma^2, \rho \sim N_n(X\beta + \gamma, \sigma^2(1 - \rho)I_n)$ where $\beta = (\beta_0, \beta_1)^T$ and β_1 is the coefficient of smoking prevalence. Similar to the simulation examples, we place a CAR prior on ϕ by setting $V_\phi^{-1} = c(D_W - \alpha W)$, where the neighbor and adjacency matrices are computed using the subset of U.S. counties, $\alpha = 0.99$, and $c = 0.3762$. We treat ρ as an unknown parameter and specify the joint prior as $\pi(\beta, \gamma, \sigma^2, \rho) = N_n(\gamma | 0, \sigma^2 \rho V_\phi) \times \text{IG}(\sigma^2 | a_{\sigma^2}, b_{\sigma^2}) \times \text{PC}(\rho | \lambda_\rho)$, where $a_{\sigma^2} = 0.1$ and $b_{\sigma^2} = 0.1$. Although the set of regions here differs slightly from the simulation example, we also set $\lambda_\rho = 0.0335$ since it approximately satisfies $\mathbb{P}(\rho \leq 0.5) = \frac{2}{3}$.

After 10,000 burn-in samples, we draw 30,000 samples from of the posterior of $\{\beta, \gamma, \sigma^2, \rho\}$ using Algorithm 1. Table 1 presents 95% credible intervals for the non-spatial effect parameters. The credible interval of ρ suggests that we are able to learn effectively about ρ and the CAR spatial model explains a majority of the variance in the data.

We detect spatial disparities using the ϵ -difference framework in Section 3. For this dataset, we denote the set of all $K = 8,793$ pairs of neighboring counties as $L = \{(i, j) : i < j, i \sim j\}$ and

Parameter	Description	Mean	95% Credible Interval
β_0	Intercept	9.57	(6.073, 13.205)
β_1	Smoking prevalence	2.24	(2.117, 2.357)
σ^2	Total variance	114.47	(101.506, 131.105)
ρ	Spatial proportion of variance	0.78	(0.704, 0.86)

TABLE 1. Posterior summaries of non-spatial effect parameters.

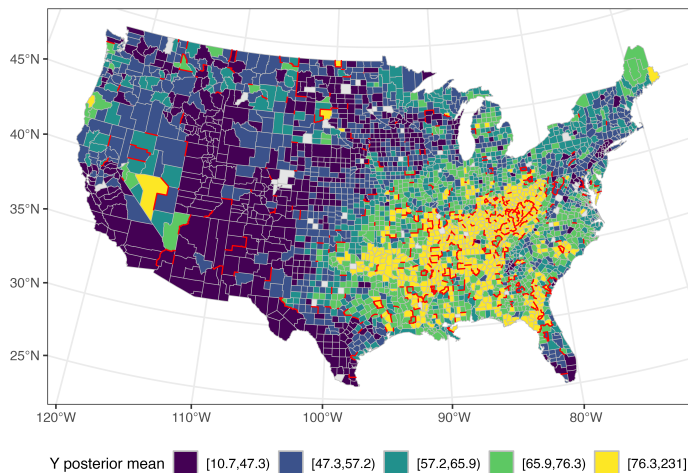


FIGURE 6. Map of posterior predictive means of lung cancer mortality rates. Red lines correspond to disparities between neighboring counties with difference threshold $\epsilon_{CE} = 0.928$ and Bayesian FDR tolerance $\delta = 0.05$.

ϵ -difference probabilities of the form $v_{ij}(\epsilon) = \mathbb{P}\left(\frac{|\phi_i - \phi_j|}{\sqrt{a_{ij}^T \text{Var}(\phi | y, \sigma^2, \rho) a_{ij}}} > \epsilon \mid y\right)$ for all $(i, j) \in L$. We select the difference threshold ϵ by minimizing the conditional entropy loss in (18), which yields $\epsilon_{CE} = 0.928$. For this analysis, we set a maximum allowable Bayesian FDR of $\delta = 0.05$, compute $t_\star = 0.882$ using (17) and report 731 county boundaries exhibiting spatial disparities.

The posterior predictive means and detected disparities are mapped in Figure 6. The reported disparities mostly lie in relatively high risk states (KY, GA, TN, WV, MS, MS, MO, VA), where several county mortality rate estimates are in the upper quintile with a large range, suggesting prevalence of health inequities in the local county scale. This aligns with our intuition that detected disparities would be more abundant in higher-risk regions with more pronounced geographic variation. The full list of 731 detected difference boundaries ranked by their corresponding difference probabilities are available in Table S1.

6. DISCUSSION

Our ϵ -based difference boundary detection is considerably simpler to implement, and interpret, than Bayesian non-parametric approaches (Gao et al., 2023; Li et al., 2015). We are able to stabilize the difference probabilities with respect to ϵ , which allows public health officials to report, say, the top fifty disparities between neighboring counties in a robust manner. We could also define a difference boundary based on the posterior predictive distribution rather than the posterior distribution of the random effects. We provide some insights in Section S6 and establish stabilized rankings for the exact conjugate model. This may be preferred in public health practice because of its interpretation in terms of the health outcome itself, but such differences will conflate disparities attributed to space with non-spatial explanatory variables or risk factors. Future areas of investigation will include (i) the impact of spatial confounding on ϵ -based boundary detection, and (ii) extending our framework to multivariate modeling with dependent areal outcomes.

7. SUPPLEMENTARY MATERIALS

Supplementary materials contains additional analysis on the behavior of the DIC and WAIC as $\rho \rightarrow 1^-$, formulation of an ϵ -difference probability on the modeled response level, and the full list of spatial disparities in the data analysis example. All computer programs required to reproduce the simulation and data analysis in this manuscript are available at https://github.com/Ky-Wu/bayesian_spatial_health_disparities.

REFERENCES

- L. Aiello and S. Banerjee. Detecting spatial health disparities using disease maps, 2023. URL <https://arxiv.org/abs/2309.02086>.
- S. Banerjee, B. P. Carlin, and A. E. Gelfand. *Hierarchical Modeling and Analysis for Spatial Data*. Number 135 in Monographs on Statistics and Applied Probability. CRC Press, Taylor & Francis Group, Boca Raton, second edition, 2015. ISBN 978-1-4398-1917-3.
- Y. Benjamini and Y. Hochberg. Controlling the False Discovery Rate: A Practical and Powerful Approach to Multiple Testing. *Journal of the Royal Statistical Society: Series B (Methodological)*, 57(1):289–300, 1995. ISSN 2517-6161. doi: 10.1111/j.2517-6161.1995.tb02031.x.
- J. Besag, J. York, and A. Mollié. Bayesian image restoration, with two applications in spatial statistics. *Annals of the Institute of Statistical Mathematics*, 43(1):1–20, Mar. 1991. ISSN 1572-9052. doi: 10.1007/BF00116466.
- D. M. Blei, A. Kucukelbir, and J. D. McAuliffe. Variational Inference: A Review for Statisticians. *Journal of the American Statistical Association*, 112(518):859–877, Apr. 2017. ISSN 0162-1459, 1537-274X. doi: 10.1080/01621459.2017.1285773.

- F. Corpas-Burgos and M. A. Martinez-Beneito. On the use of adaptive spatial weight matrices from disease mapping multivariate analyses. *Stochastic Environmental Research and Risk Assessment*, 34:531–544, 2020.
- L. Dwyer-Lindgren, A. H. Mokdad, T. Srebotnjak, A. D. Flaxman, G. M. Hansen, and C. J. Murray. Cigarette smoking prevalence in US counties: 1996-2012. *Population Health Metrics*, 12(1):5, Mar. 2014. ISSN 1478-7954. doi: 10.1186/1478-7954-12-5.
- A. Fischer, R. E. Gaunt, G. Reinert, and Y. Swan. Normal approximation for the posterior in exponential families, Jan. 2025.
- M. C. Fitzpatrick, E. L. Preisser, A. Porter, J. Elkinton, L. A. Waller, B. P. Carlin, and A. M. Ellison. Ecological boundary detection using bayesian areal wombling. *Ecology*, 91(12): 3448–3455, 2010. doi: <https://doi.org/10.1890/10-0807.1>. URL <https://esajournals.onlinelibrary.wiley.com/doi/abs/10.1890/10-0807.1>.
- L. Gao, S. Banerjee, and B. Ritz. Spatial Difference Boundary Detection for Multiple Outcomes Using Bayesian Disease Mapping. *Biostatistics*, 24(4):922–944, Oct. 2023. ISSN 1465-4644. doi: 10.1093/biostatistics/kxac013.
- A. Gelman. Prior distributions for variance parameters in hierarchical models (comment on article by Browne and Draper). *Bayesian Analysis*, 1(3):515–534, Sept. 2006. ISSN 1936-0975, 1931-6690. doi: 10.1214/06-BA117A.
- A. Gelman, J. Hwang, and A. Vehtari. Understanding predictive information criteria for Bayesian models. *Statistics and Computing*, 24(6):997–1016, Nov. 2014. ISSN 1573-1375. doi: 10.1007/s11222-013-9416-2.
- T. Hanson, S. Banerjee, P. Li, and A. McBean. Spatial boundary detection for areal counts. In *Nonparametric Bayesian Inference in Biostatistics*, pages 377–399. Springer, 2015.
- G. M. Jacquez and D. A. Greiling. Geographic boundaries in breast, lung and colorectal cancers in relation to exposure to air toxics in long island, new york. *International Journal of Health Geographics*, 2(1):1–22, 2003a.
- G. M. Jacquez and D. A. Greiling. Local clustering in breast, lung and colorectal cancer in long island, new york. *International Journal of Health Geographics*, 2(1):1–12, 2003b.
- E. T. Jaynes. Information Theory and Statistical Mechanics. *Physical Review*, 106(4):620–630, May 1957. ISSN 0031-899X. doi: 10.1103/PhysRev.106.620.
- A. B. Lawson. *Statistical methods in spatial epidemiology*. John Wiley & Sons, 2013.
- B. Lawson, Andrew, S. Banerjee, R. Haining, and D. Ugarte, Maria. *Handbook of Spatial Epidemiology*. CRC press, Boca Raton, FL, 2016.
- D. Lee and R. Mitchell. Boundary detection in disease mapping studies. *Biostatistics*, 13(3): 415–426, July 2012. ISSN 1465-4644. doi: 10.1093/biostatistics/kxr036.
- P. Li, S. Banerjee, and A. M. McBean. Mining boundary effects in areally referenced spatial data using the bayesian information criterion. *Geoinformatica*, 15(3):435–454, 2011.

- P. Li, S. Banerjee, B. P. Carlin, and A. M. McBean. Bayesian areal wombling using false discovery rates. *Statistics and its Interface*, 5(2):149–158, 2012.
- P. Li, S. Banerjee, T. A. Hanson, and A. M. McBean. Bayesian models for detecting difference boundaries in areal data. *Statistica Sinica*, 25(1):385, 2015.
- H. Lu and B. P. Carlin. Bayesian areal wombling for geographical boundary analysis. *Geographical Analysis*, 37(3):265–285, 2005.
- H. Lu, C. S. Reilly, S. Banerjee, and B. P. Carlin. Bayesian areal wombling via adjacency modeling. *Environmental and ecological statistics*, 14:433–452, 2007.
- H. Ma and B. P. Carlin. Bayesian multivariate areal wombling for multiple disease boundary analysis. *Bayesian Analysis*, 2(2):281–302, 2007.
- H. Ma, B. P. Carlin, and S. Banerjee. Hierarchical and joint site-edge methods for medicare hospice service region boundary analysis. *Biometrics*, 66(2):355–364, 2010.
- Z. Ma and G. Chen. Bayesian methods for dealing with missing data problems. *Journal of the Korean Statistical Society*, 47(3):297–313, Sept. 2018. ISSN 2005-2863. doi: 10.1016/j.jkss.2018.03.002.
- A. H. Mokdad, L. Dwyer-Lindgren, C. Fitzmaurice, R. W. Stubbs, A. Bertozzi-Villa, C. Morozoff, R. Charara, C. Allen, M. Naghavi, and C. J. L. Murray. Trends and Patterns of Disparities in Cancer Mortality Among US Counties, 1980-2014. *JAMA*, 317(4):388–406, Jan. 2017. ISSN 0098-7484. doi: 10.1001/jama.2016.20324.
- P. Müller, G. Parmigiani, C. Robert, and J. Rousseau. Optimal Sample Size for Multiple Testing. *Journal of the American Statistical Association*, 99(468):990–1001, Dec. 2004. ISSN 0162-1459. doi: 10.1198/016214504000001646.
- P. Müller, G. Parmigiani, and K. Rice. FDR and Bayesian Multiple Comparisons Rules. In *Bayesian Statistics 8: Proceedings of the Eighth Valencia International Meeting June 2–6, 2006*. Oxford University Press, July 2007. ISBN 978-0-19-921465-5. doi: 10.1093/oso/9780199214655.003.0014.
- J. S. Rao. *Statistical Methods in Health Disparity Research*. Chapman & Hall/CRC, Boca Raton, FL, 2023.
- Q. Ren, S. Banerjee, A. O. Finley, and J. S. Hodges. Variational Bayesian methods for spatial data analysis. *Computational Statistics & Data Analysis*, 55(12):3197–3217, 2011. ISSN 0167-9473. doi: <https://doi.org/10.1016/j.csda.2011.05.021>. URL <https://www.sciencedirect.com/science/article/pii/S0167947311002003>.
- A. Riebler, S. H. Sørbye, D. Simpson, and H. Rue. An intuitive Bayesian spatial model for disease mapping that accounts for scaling. *Statistical Methods in Medical Research*, 25(4):1145–1165, Aug. 2016. ISSN 0962-2802. doi: 10.1177/0962280216660421.
- D. B. Rubin. Inference and missing data. *Biometrika*, 63(3):581–592, Dec. 1976. ISSN 0006-3444. doi: 10.1093/biomet/63.3.581.

- T. Salimans and D. A. Knowles. Fixed-Form Variational Posterior Approximation through Stochastic Linear Regression. *Bayesian Analysis*, 8(4), Dec. 2013. ISSN 1936-0975. doi: 10.1214/13-BA858.
- J. G. Scott and J. O. Berger. An exploration of aspects of Bayesian multiple testing. *Journal of Statistical Planning and Inference*, 136(7):2144–2162, July 2006. ISSN 0378-3758. doi: 10.1016/j.jspi.2005.08.031.
- G. A. Seber and A. J. Lee. Hypothesis Testing. In *Linear Regression Analysis*, chapter 4, pages 97–118. John Wiley & Sons, Ltd, 2003. ISBN 978-0-471-72219-9. doi: 10.1002/9780471722199.ch4.
- C. E. Shannon. A Mathematical Theory of Communication. *Bell System Technical Journal*, 27(3): 379–423, July 1948. ISSN 00058580. doi: 10.1002/j.1538-7305.1948.tb01338.x.
- A. H. Shreves, I. D. Buller, E. Chase, H. Creutzfeldt, J. A. Fisher, B. I. Graubard, R. N. Hoover, D. T. Silverman, S. S. Devesa, and R. R. Jones. Geographic Patterns in U.S. Lung Cancer Mortality and Cigarette Smoking. *Cancer Epidemiology, Biomarkers & Prevention*, 32(2):193–201, Feb. 2023. ISSN 1055-9965. doi: 10.1158/1055-9965.EPI-22-0253.
- D. Simpson, H. Rue, A. Riebler, T. G. Martins, and S. H. Sørbye. Penalising Model Component Complexity: A Principled, Practical Approach to Constructing Priors. *Statistical Science*, 32(1): 1–28, 2017. ISSN 0883-4237.
- D. J. Spiegelhalter, N. G. Best, B. P. Carlin, and A. Van Der Linde. Bayesian measures of model complexity and fit. *Journal of the Royal Statistical Society: Series B (Statistical Methodology)*, 64(4):583–639, 2002. ISSN 1467-9868. doi: 10.1111/1467-9868.00353.
- L. Waller and B. Carlin. Disease mapping. In A. E. Gelfand, P. Diggle, P. Guttorp, and M. Fuentes, editors, *Handbook Of Spatial Statistics*, page 217–243. CRC Press, Boca Raton, FL, 2010.
- L. A. Waller and C. A. Gotway. *Applied spatial statistics for public health data*, volume 368. John Wiley & Sons, 2004.
- S. Watanabe. Asymptotic Equivalence of Bayes Cross Validation and Widely Applicable Information Criterion in Singular Learning Theory. *Journal of Machine Learning Research*, 11(116): 3571–3594, 2010. ISSN 1533-7928.

APPENDIX A. PROOF OF THEOREM 1

Under the standard linear model described in Theorem 1, the p-values, $p_k = \mathbb{P} \left(t > |t_{\text{obs}}^{(k)}| \right)$, are characterized by a common t-distribution CDF evaluated at the observed t-statistics. As CDFs are monotonic functions, $p_k > p_{k'}$ if and only if $|t_{\text{obs}}^{(k)}| < |t_{\text{obs}}^{(k')}|$. Next, it is well known that when $\pi(\beta, \sigma^2) \propto \pi(\sigma^2)$, then $\beta | y, \sigma^2 \sim N \left(\hat{\beta}, \sigma^2 (X^T V_y^{-1} X)^{-1} \right)$, where $\hat{\beta} = (X^T V_y^{-1} X)^{-1} X^T V_y^{-1} y$ is the

generalized least squares estimate. We have that for any $\epsilon > 0$, $\sigma^2 > 0$,

$$\begin{aligned} \mathbb{P}\left(\frac{|c_k^\top \beta|}{\sigma \sqrt{c_k^\top M c_k}} > \epsilon \mid y, \sigma^2\right) &= 1 - \mathbb{P}\left(-\epsilon \leq \frac{c_k^\top \beta}{\sigma \sqrt{c_k^\top (X^\top V_y^{-1} X)^{-1} c_k}} \leq \epsilon \mid y, \sigma^2\right) \\ &= \Phi\left(-\epsilon + \frac{c_k^\top \hat{\beta}}{\sigma \sqrt{c_k^\top (X^\top V_y^{-1} X)^{-1} c_k}}\right) + \Phi\left(-\epsilon - \frac{c_k^\top \hat{\beta}}{\sigma \sqrt{c_k^\top (X^\top V_y^{-1} X)^{-1} c_k}}\right) \\ &= \Phi\left(\epsilon - \frac{\hat{\sigma}}{\sigma} t_{\text{obs}}^{(k)}\right) + \Phi\left(\epsilon + \frac{\hat{\sigma}}{\sigma} t_{\text{obs}}^{(k)}\right) \end{aligned}$$

where Φ denotes the standard normal CDF. We now use the following lemma:

Lemma 1. *Let $\epsilon > 0$, $c > 0$, $G : \mathbb{R} \rightarrow [0, 1]$ be a function such that $G'(x)$ is symmetric around zero and strictly decreasing in $|x|$, and $h : \mathbb{R} \rightarrow [0, 1]$ be given by $h(x) = G(\epsilon - cx) + G(\epsilon + cx)$ for all $x \in \mathbb{R}$. Then, h is symmetric and if $x, y \in \mathbb{R}$, $h(x) > h(y)$ if and only if $|x| > |y|$.*

Proof. By assumption, $h'(x) = cG'(\epsilon + cx) - cG'(\epsilon - cx)$. Since $G'(x)$ is strictly decreasing in $|x|$, then if $x < 0$, $|\epsilon + cx| < |\epsilon - cx|$ and thus $h'(x) > 0$. If $x > 0$, then $|\epsilon + cx| > |\epsilon - cx|$, so $h'(x) < 0$. Furthermore, $h(-x) = G(\epsilon + cx) + G(\epsilon - cx) = h(x)$, so h is symmetric and strictly increasing in $|x|$, which proves the claim.

By Lemma 1, since $\hat{\sigma}/\sigma > 0$ and the standard normal PDF $\Phi'(x)$ is symmetric around zero and strictly decreasing in $|x|$, then

$$\mathbb{P}\left(\frac{|c_k^\top \beta|}{\sigma \sqrt{c_k^\top M c_k}} > \epsilon \mid y, \sigma^2\right) < \mathbb{P}\left(\frac{|c_{k'}^\top \beta|}{\sigma \sqrt{c_{k'}^\top M c_{k'}}} > \epsilon \mid y, \sigma^2\right) \iff |t_{\text{obs}}^{(k)}| < |t_{\text{obs}}^{(k')}|$$

for any $\epsilon > 0$, $\sigma^2 > 0$. If $|t_{\text{obs}}^{(k)}| < |t_{\text{obs}}^{(k')}|$, integrating out σ^2 preserves the order as

$$\begin{aligned} v_k(\epsilon) &= \mathbb{P}\left(\frac{|c_k^\top \beta|}{\sigma \sqrt{c_k^\top M c_k}} > \epsilon \mid y\right) = \int_0^\infty \mathbb{P}\left(\frac{|c_k^\top \beta|}{\sigma \sqrt{c_k^\top M c_k}} > \epsilon \mid y, \sigma^2\right) \pi(\sigma^2 \mid y) d\sigma^2 \\ &< \int_0^\infty \mathbb{P}\left(\frac{|c_{k'}^\top \beta|}{\sigma \sqrt{c_{k'}^\top M c_{k'}}} > \epsilon \mid y, \sigma^2\right) \pi(\sigma^2 \mid y) d\sigma^2 = \mathbb{P}\left(\frac{|c_{k'}^\top \beta|}{\sigma \sqrt{c_{k'}^\top M c_{k'}}} > \epsilon \mid y\right) = v_{k'}(\epsilon) \end{aligned}$$

which shows that $|t_{\text{obs}}^{(k)}| < |t_{\text{obs}}^{(k')}|$ implies $v_k(\epsilon) < v_{k'}(\epsilon)$ for all $\epsilon > 0$. If $v_k(\epsilon) < v_{k'}(\epsilon)$ for all $\epsilon > 0$, then this implies there exists $\epsilon > 0$, $\sigma^2 > 0$ such that $\mathbb{P}\left(\frac{|c_k^\top \beta|}{\sigma \sqrt{c_k^\top M c_k}} > \epsilon \mid y, \sigma^2\right) <$

$\mathbb{P}\left(\frac{|c_{k'}^T \beta|}{\sigma \sqrt{c_{k'}^T M c_{k'}}} > \epsilon \mid y, \sigma^2\right)$, which implies $|t_{\text{obs}}^{(k)}| < |t_{\text{obs}}^{(k')}|$ by the above argument. Therefore,

$$p_k > p_{k'} \iff |t_{\text{obs}}^{(k)}| < |t_{\text{obs}}^{(k')}| \iff \mathbb{P}\left(\frac{|c_k^T \beta|}{\sigma \sqrt{c_k^T M c_k}} > \epsilon \mid y, \sigma^2\right) < \mathbb{P}\left(\frac{|c_{k'}^T \beta|}{\sigma \sqrt{c_{k'}^T M c_{k'}}} > \epsilon \mid y, \sigma^2\right)$$

for all $\sigma^2 > 0$ and $\epsilon > 0$. The above inequality holds if and only if $v_k(\epsilon) < v_{k'}(\epsilon) \forall \epsilon > 0$.

APPENDIX B. PROOF OF THEOREM 2

The posterior conditional distributions from (2) are given by (3). Thus, $\pi(\gamma_\star | y, \rho, \sigma^2) = N_{n+p}(\gamma_\star | M_\star m_\star, \sigma^2 M_\star)$. For all $k = 1, \dots, K$, denote $\alpha_k = \frac{c_k^T M_\star m_\star}{\sqrt{c_k^T (X_\star^T V_{y_\star}^{-1} X_\star)^{-1} c_k}}$. Then,

$$\begin{aligned} \mathbb{P}\left(\frac{|c_k^T \gamma_\star|}{\sigma \sqrt{c_k^T (X_\star^T V_{y_\star}^{-1} X_\star)^{-1} c_k}} > \epsilon \mid y, \rho, \sigma^2\right) &= 1 - \mathbb{P}\left(-\epsilon \leq \frac{c_k^T \gamma_\star}{\sigma \sqrt{c_k^T (X_\star^T V_{y_\star}^{-1} X_\star)^{-1} c_k}} \leq \epsilon \mid y, \rho, \sigma^2\right) \\ &= \Phi\left(-\epsilon + \frac{\alpha_k}{\sigma}\right) + \Phi\left(-\epsilon - \frac{\alpha_k}{\sigma}\right). \end{aligned}$$

By Lemma 1, for any $k \neq k'$, $|\alpha_k| < |\alpha_{k'}|$ if and only if $\mathbb{P}\left(\frac{|c_k^T \gamma_\star|}{\sigma \sqrt{c_k^T (X_\star^T V_{y_\star}^{-1} X_\star)^{-1} c_k}} > \epsilon \mid y, \rho, \sigma^2\right) <$

$\mathbb{P}\left(\frac{|c_{k'}^T \gamma_\star|}{\sigma \sqrt{c_{k'}^T (X_\star^T V_{y_\star}^{-1} X_\star)^{-1} c_{k'}}} > \epsilon \mid y, \rho, \sigma^2\right)$ for all $\sigma^2 > 0, \epsilon > 0$. If there exists $\epsilon_\star > 0$ such that

$h_k(\epsilon_\star; \rho) < h_{k'}(\epsilon_\star; \rho)$, then there exists $\sigma^2 > 0$ such that $\mathbb{P}\left(\frac{|c_k^T \gamma_\star|}{\sigma \sqrt{c_k^T (X_\star^T V_{y_\star}^{-1} X_\star)^{-1} c_k}} > \epsilon_\star \mid y, \rho, \sigma^2\right) <$

$\mathbb{P}\left(\frac{|c_{k'}^T \gamma_\star|}{\sigma \sqrt{c_{k'}^T (X_\star^T V_{y_\star}^{-1} X_\star)^{-1} c_{k'}}} > \epsilon_\star \mid y, \rho, \sigma^2\right)$, which implies $|\alpha_k| < |\alpha_{k'}|$. Thus, for any $\epsilon > 0$,

$$\begin{aligned} h_k(\epsilon; \rho) &= \int_0^\infty \mathbb{P}\left(\frac{|c_k^T \gamma_\star|}{\sigma \sqrt{c_k^T (X_\star^T V_{y_\star}^{-1} X_\star)^{-1} c_k}} > \epsilon \mid y, \rho, \sigma^2\right) \pi(\sigma^2 | y, \rho) d\sigma^2 \\ &< \int_0^\infty \mathbb{P}\left(\frac{|c_{k'}^T \gamma_\star|}{\sigma \sqrt{c_{k'}^T (X_\star^T V_{y_\star}^{-1} X_\star)^{-1} c_{k'}}} > \epsilon \mid y, \rho, \sigma^2\right) \pi(\sigma^2 | y, \rho) d\sigma^2 = h_{k'}(\epsilon; \rho), \end{aligned}$$

which completes the proof.

SUPPLEMENTARY MATERIAL FOR ASSESSING SPATIAL DISPARITIES: A BAYESIAN LINEAR REGRESSION APPROACH

KYLE LIN WU AND SUDIPTO BANERJEE

S1. METROPOLIS WITHIN GIBBS SAMPLING ALGORITHM FOR BYM2 MODEL

We present a Metropolis within Gibbs sampling algorithm for obtaining posterior samples of $\{\beta, \gamma, \sigma^2, \rho\}$ under the model given by (1) and prior $\pi(\beta, \gamma, \sigma^2, \rho) = N_n(\gamma | 0, \sigma^2 \rho V_\phi) \times \text{IG}(\sigma^2 | a_{\sigma^2}, b_{\sigma^2}) \times \text{PC}(\rho | \lambda_\rho, V_\phi)$. Algorithm 1 calls simultaneous reduction on V_ϕ^{-1} and $I - H$ to efficiently compute posterior samples of $\Delta_k = \frac{c_k^T \phi}{\sqrt{c_k^T \text{Var}(\phi | y, \sigma^2, \rho) c_k}}$ for estimation of ϵ -difference probabilities through (10).

Algorithm 1: Metropolis within Gibbs sampling of posterior of $(\beta, \gamma, \sigma^2, \rho)$ in BYM2 Model with flat β prior and PC ρ prior

Given $y, X, R = \text{chol}(X^T X), I - H, V_\phi^{-1}, a_{\sigma^2}, b_{\sigma^2}, \lambda_\rho, \beta^{(0)}, \gamma^{(0)}, \sigma^{2(0)}, \rho^{(0)}, c_1, \dots, c_K$:

Set $U, D, P, \Lambda \leftarrow \text{simulReduce}(V_\phi^{-1}, I - H)$.

Precompute $m_1 \leftarrow X^T y$.

for $k = 1, \dots, K$ **do**

 | Set $\omega_k \leftarrow U^T c_k$.

for $t = 1, \dots, T$ **do**

 | Set $\beta^{(t)} \leftarrow \text{updateBeta}(\gamma^{(t-1)}, \sigma^{2(t-1)}, \rho^{(t-1)})$.

 | Set $\gamma^{(t)} \leftarrow \text{updateGamma}(\beta^{(t)}, \sigma^{2(t-1)}, \rho^{(t-1)})$.

 | Set $r^{2(t)} \leftarrow \|y - X\beta^{(t)} - \gamma^{(t)}\|^2$.

 | Set $\sigma^{2(t)} \leftarrow \text{updateSigmaSq}(\rho^{(t-1)}, r^{2(t)})$.

 | Set $\rho^{(t)} \leftarrow \text{MHupdateRho}(\gamma^{(t)}, \sigma^{2(t)}, \rho^{(t-1)}, r^{2(t)})$.

 | Set $\phi^{(t)} \leftarrow \gamma^{(t)} / (\sigma^{(t)} \sqrt{\rho^{(t)}})$.

for $k = 1, \dots, K$ **do**

 | Set $\Delta_k^{(t)} = \left(\omega_k^T \text{diag} \left(\frac{1 - \rho^{(t)}}{1 + \rho^{(t)}(d_i - 1)} \right) \omega_k \right)^{-1/2} c_k^T \phi^{(t)}$.

function `simulReduce`(A, B):

 | Solve spectral decomposition $A = P\Lambda P^T$ and set $A^{-1/2} \leftarrow P\Lambda^{-1/2}P^T$.

 | Solve spectral decomposition $A^{-1/2}BA^{-1/2} = CDC^T$ and set $U \leftarrow A^{-1/2}C$.

return U, D, P, Λ .

Date: March 18, 2025.

Algorithm 2: Update steps for Metropolis within Gibbs sampling of posterior of $(\beta, \gamma, \sigma^2, \rho)$ in BYM2 Model with flat β prior and PC ρ prior

Given $y, X, R = \text{chol}(X^T X), V_\phi^{-1}, m_1 = X^T y, P, \Lambda = \text{diag}(\lambda_1, \dots, \lambda_n), a_{\sigma^2}, b_{\sigma^2}, \lambda_\rho$:

function updateBeta(γ, σ^2, ρ):

for $i = 1, \dots, p$ **do**

 | Sample $z_i \sim N(0, \sigma^2(1 - \rho))$.

 Set $v_p \leftarrow \text{forwardsolve}(R^T, m_1 - X^T \gamma)$; $\beta \leftarrow \text{backsolve}(R, v_p + z)$.

return β .

function updateGamma(β, σ^2, ρ):

 Set $v_n \leftarrow y - X\beta$.

 Update $v_n \leftarrow \text{diag}\left(\frac{\rho}{\rho + (1-\rho)\lambda_i}\right) P^T v_n$.

for $i = 1, \dots, n$ **do**

 | Sample $z_i \sim N(0, \sigma^2)$.

 Set $\gamma \leftarrow P\left(v_n + \text{diag}\left(\sqrt{\frac{\rho(1-\rho)}{\rho + \lambda_i(1-\rho)}}\right) z\right)$.

return γ .

function updateSigmaSq(ρ, r^2):

 Sample $\tau^2 \sim \Gamma\left(a_{\sigma^2} + \frac{n}{2}, b_{\sigma^2} + \frac{r^2}{2(1-\rho)}\right)$; set $\sigma^2 \leftarrow 1/\tau^2$.

return σ^2 .

function MHupdateRho($\gamma, \sigma^2, \rho, r^2$):

 Initialize $\rho_\star \leftarrow 1$.

while $\rho_\star \geq 1$ **do**

 | Sample $\tau^2 \sim \Gamma\left(\frac{n}{2}, \frac{r^2}{2\sigma^2}\right)$; set $\rho_\star \leftarrow 1 - 1/\tau^2$.

 Set $c_1 \leftarrow \sqrt{\sum_{i=1}^n \left(\frac{\rho}{\lambda_i} - \log\left(\frac{\rho}{\lambda_i} + (1 - \rho)\right)\right)} - n\rho$.

 Set $c_2 \leftarrow \sqrt{\sum_{i=1}^n \left(\frac{\rho_\star}{\lambda_i} - \log\left(\frac{\rho_\star}{\lambda_i} + (1 - \rho_\star)\right)\right)} - n\rho_\star$.

 Set $\alpha_{MH} \leftarrow \frac{n}{2} \log\left(\frac{\rho}{\rho_\star}\right) + \lambda_\rho (c_1 - c_2) + \frac{\gamma^T V_\phi^{-1} \gamma}{2\sigma^2} \left(\frac{1}{\rho} - \frac{1}{\rho_\star}\right)$.

 Sample $u \sim \text{Unif}(0, 1)$.

if $\log(u) \leq \alpha_{MH}$ **then return** ρ_\star .

else return ρ .

S2. SIMULATION COMPARISON WITH ARDP

S2.1. Data Generation. We compare difference boundary classification performance between our ϵ -difference approach and the areally-referenced Dirichlet process (ARDP) method introduced by Li et al. (2015) and expanded to the multivariate setting in Gao et al. (2023) in simulated datasets on a map of the Californian counties.

To create a reference dataset, we first draw $z \sim N_n(0_n, \Sigma)$, where Σ is a exponential covariance kernel such that $\Sigma_{ij} = \exp(-d_{ij}/150)$ where d_{ij} is the Great Circle distance between the centroids of regions i and j in kilometres. We divide the components z_1, \dots, z_n into quintiles and replace each component with the mean of the corresponding quintile. The resulting spatial effects ϕ are mapped in the left panel of Figure S1. Out of 139 total, there are 90 boundaries (i, j) where $\phi_i \neq \phi_j$, which we label as the true difference boundaries. We then generate 50 datasets $\{X^{(i)}, y^{(i)}\}$ by generating covariates $X^{(i)} = (1_n, x^{(i)})$, $x^{(i)} \sim N_n(0, I_n)$ and the response $y^{(i)} \sim N_n(X\beta + \gamma, \sigma^2(1 - \rho)I_n)$ with $\gamma = \sigma^2\rho\phi$, $\rho = 0.9$, $\sigma^2 = 5$, and $\beta = (2, 5)^\top$.

For both methods, we compute difference probabilities over L , the set of all boundaries between Californian counties. For the ϵ -difference method, we employ the BYM2 model in (1) with the prior $\pi(\beta, \gamma, \sigma^2, \rho) = N_n(\gamma | 0_n, V_\phi) \times \text{IG}(\sigma^2 | 0.1, 0.1) \times \text{Beta}(\rho | 1, 1)$. We use a spatial CAR prior with $V_\phi^{-1} = c(D_W - \alpha W)$ constructed using the adjacency relations of the Californian counties, $\alpha = 0.99$, and $c = 0.8352$. For each dataset, we draw $20,000 \times 4$ chains = 80,000 posterior samples of $(\beta, \gamma, \rho, \sigma^2)$ after 40,000 burn-in samples using Hamiltonian Monte Carlo (RSt, 2023), obtain ϵ_{CE} by minimizing (18), and estimate the difference probabilities $\{v_{ij}(\epsilon_{CE})\}_{(i,j) \in L}$ using (10).

S2.2. ARDP Specification. The ARDP model builds spatial dependence through a Markov random field on a latent component and imbues the spatial effects with a probability distribution. Following the notation of Li et al. (2015), we write the ARDP model as

$$\begin{aligned}
Y | \beta, \gamma, \sigma^2 &\sim N_n(X\beta + \gamma, \sigma^2 I_n), \quad \gamma \sim G_n, \quad G_n = \sum_{u_1, \dots, u_n} \pi_{u_1, \dots, u_n} \delta_{\zeta_{u_1}} \cdots \delta_{\zeta_{u_n}}; \\
\pi_{u_1, \dots, u_n} &= \mathbb{P} \left(\sum_{k=1}^{u_1-1} p_k < F^{(1)}(\phi_1) < \sum_{k=1}^{u_1} p_k, \dots, \sum_{k=1}^{u_n-1} p_k < F^{(n)}(\phi_n) < \sum_{k=1}^{u_n} p_k \right); \\
\zeta &\sim N_K(0, \sigma_s^2), \quad p_1 = V_1, \quad p_j = V_j \prod_{k < j} (1 - V_k), \quad V_j \stackrel{i.i.d.}{\sim} \text{Beta}(1, \alpha_V), \quad \phi \sim N_n(0, W_\phi),
\end{aligned} \tag{1}$$

where $F^{(i)}(\cdot)$ is the CDF of the marginal component ϕ_i , u_1, \dots, u_n are indices sampled from $\{1, \dots, N\}$, and $\{p_1, \dots, p_K\}$ are the stick-breaking weights truncated to K clusters. The spatial components ϕ follow a directed acyclic graphical autoregression (DAGAR) model parameterized by $\rho \in (0, 1)$, a spatial autocorrelation parameter (Datta et al., 2019). The DAGAR model requires a specific ordering of the regions $\{1, \dots, n\}$, which we construct by sorting $\delta_1 < \delta_2 < \dots < \delta_n$ where $\delta_i = L_{i,1} - L_{i,2}$ and $(L_{i,1}, L_{i,2})$ are the coordinates of a Albers projection of the i th county's centroid. Denote $N(i)$ as the set of neighbouring regions that precede i in the ordering and a_i is the number of regions in $N(i)$. Then, $W_\phi^{-1} = (I_n - B)^\top R (I_n - B)$, where $B_{ij} = 0$ if $j \notin N(i)$, $B_{ij} = \frac{\rho}{1 + (a_i - 1)\rho^2}$ for $i = 2, \dots, n$ and $j \in N(i)$, and R is a diagonal matrix with $R_{ii} = \frac{1 + (a_i - 1)\rho^2}{1 - \rho^2}$ for $i = 1, \dots, n$.

We match the simulation setting in Gao et al. (2023) by completing (1) with the prior $\pi(\beta, \sigma^2, \sigma_s^2, \rho) = N_p(\beta | 0_p, 10000I_p) \times \text{IG}(\sigma^2 | 2, 0.1) \times \text{IG}(\sigma_s^2 | 2, 1) \times \text{Unif}(\rho | 0, 0.98)$ and fixing $\alpha_V = 1$. For

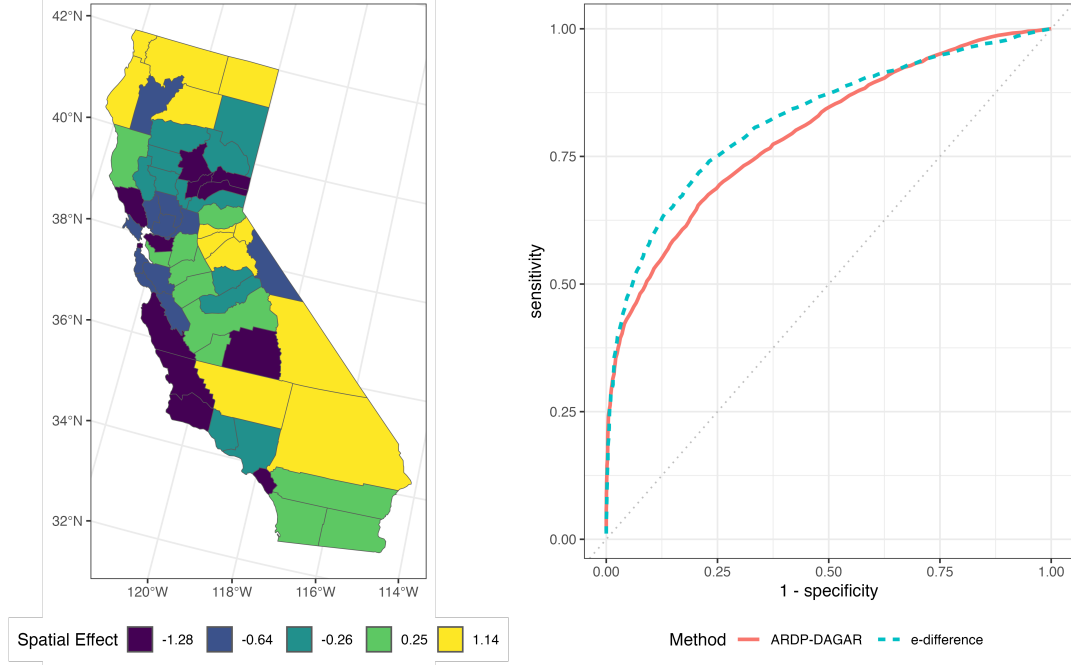


FIGURE S1. Left: simulated spatial effects ϕ . There are 90 difference boundaries separating counties with distinct spatial effects. Right: averaged ROC curves for ϵ -difference method with CAR spatial kernel and ARDP-DAGAR method.

each simulated dataset, we draw $20,000 \times 2$ chains = 40,000 samples from the joint posterior $\pi(\beta, \gamma, \sigma^2, \sigma_s^2, \phi, \rho | y)$ after 40,000 burn-in samples using the MCMC algorithm implemented in Gao et al. (2023). We use the posterior samples of γ to compute Monte Carlo estimates of the difference probabilities $w_{ij} = \mathbb{P}(\gamma_i \neq \gamma_j | y)$ for all $(i, j) \in L$.

S2.3. Results. The difference probabilities $v_{ij}(\epsilon)$ and $w_{ij}(\epsilon)$ have equivalent interpretation: a higher difference probability indicates a stronger posterior belief of (i, j) being a true difference boundary. For $T = 1, \dots, 139$, we take the top T difference probabilities as the predicted difference boundaries in each dataset, and average sensitivity and specificity across the simulated datasets for each method. As T increases, sensitivity increases but specificity decreases. The averaged ROC curve in the right panel of Figure S1 shows comparable classification performance between the two methods. The AUC for the ϵ -difference method is 0.8236, while the AUC for the ARDP-DAGAR method is 0.7963. When $T = 90$, the ϵ -difference method has an averaged sensitivity of 0.811 and specificity of 0.653, while the ARDP-DAGAR method has an averaged sensitivity of 0.784 and specificity of 0.603.

S3. SIMULATION MODEL FIT AND RANKINGS OF ϵ -DIFFERENCE PROBABILITIES WITH FIXED ρ

In Section 4.1, we simulate data using (1) over a map of U.S. counties and draw exact posterior samples of $(\beta, \gamma, \sigma^2)$ using (3) conditioned on $\rho = 0.93$. For each posterior sample

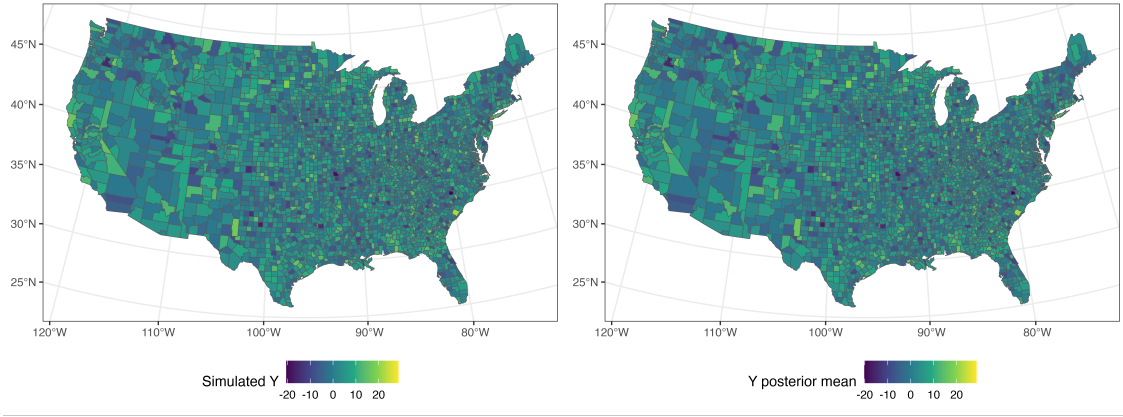


FIGURE S2. Left: simulated response data y where the spatial random effects ϕ are simulated under a scaled CAR variance structure. Right: posterior predictive means computed using 10,000 exact samples conditioned on $\rho = 0.93$.

$\{\beta^{(s)}, \gamma^{(s)}, \sigma^{2(s)}\}$, we draw one value of the predictive distribution $y_{rep}^{(s)} \sim N_n \left(X\beta^{(s)} + \gamma^{(s)}, \sigma^{2(s)}(1 - \rho^{(s)})I_n \right)$. Figure S2 shows a close match between the simulated data and posterior predictive means of each county.

Using the exact posterior samples, we compute Monte Carlo estimates of the ϵ -difference probabilities $\{h_{ij}(\epsilon)\}_{(i,j) \in L}$ and compare the rankings at $\epsilon_{CE} = 1.296$ against different threshold values $\epsilon = 0.432, 0.864, 1.944, 3.889$. The rankings in Figure S3 show slight instability in the low ranks of the rightmost graph due to imprecise Monte Carlo estimates of posterior probabilities near zero with a large difference threshold, $\epsilon = 3.889$, but otherwise support the claim of theoretically stable rankings in Theorem 2.

S4. BEHAVIOR OF DIC IN SELECTING ρ IN EXACT MODEL

In our simulations, the DIC and WAIC always suggest picking ρ arbitrarily close to 1. We show analytically that the DIC diverges to $-\infty$ as $\rho \rightarrow 1^-$.

Suppose that under the model given by (1), the prior is $\pi(\beta, \gamma, \sigma^2) = N(\gamma | 0, \sigma^2 \rho V_\phi) \times \text{IG}(\sigma^2 | a_{\sigma^2}, b_{\sigma^2})$ and consider the modeled response $Y | \beta, \gamma, \sigma^2, \rho \sim N(X\beta + \gamma, \sigma^2(1 - \rho))$. Assume $\rho \in [0, 1]$ and positive definite V_ϕ^{-1} are known. Denote $\gamma_\star = (\beta^\top, \gamma^\top)^\top$. Then, by the calculations done in Section 2.1, $\gamma_\star | y, \sigma^2, \rho \sim N(M_\star m_\star, \sigma^2 M_\star)$ and $\sigma^2 | y, \rho \sim \text{IG}(a_n, b_n)$ where $a_n = a_{\sigma^2} + \frac{n}{2}$, $b_n = b_{\sigma^2} + \frac{1}{2} \left(\frac{y^\top y}{1 - \rho} - m_\star^\top M_\star m_\star \right)$, $M_\star = \left(X_\star^\top V_{y_\star}^{-1} X_\star \right)^{-1}$, and $m_\star = X_\star^\top V_{y_\star}^{-1} y_\star = \left(\frac{1}{1 - \rho} y^\top X, \frac{1}{1 - \rho} y^\top \right)^\top$.

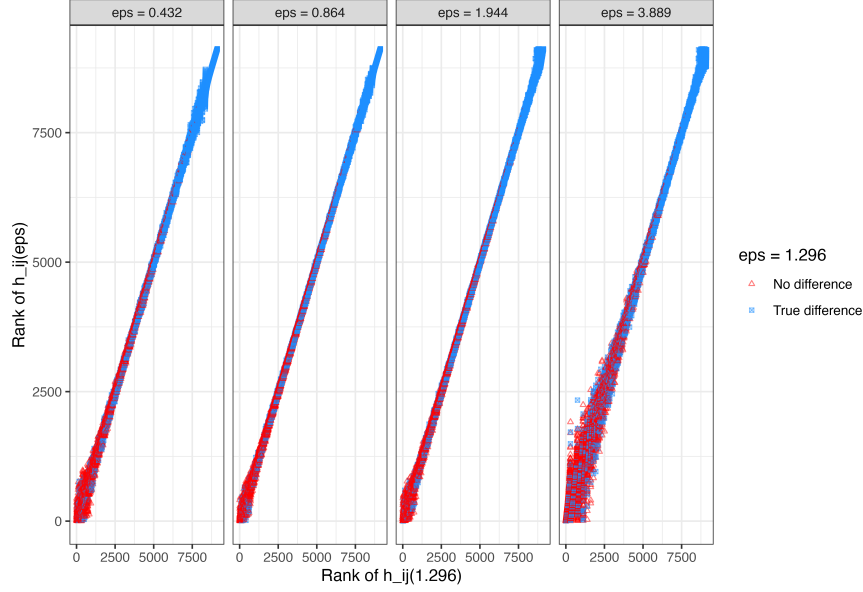


FIGURE S3. Rankings of the simulated difference probabilities $\{h_{ij}(\epsilon)\}_{(i,j) \in L}$ for $\epsilon = 0.432, 0.864, 1.944, 3.889$ versus rankings of $\{h_{ij}(\epsilon_{CE})\}_{(i,j) \in L}$ when conditioning on the true value of ρ . Disparities according to the true values of ϕ and ρ are shown in blue.

The posterior means are given by $\hat{\gamma}_\star = M_\star m_\star$, $\hat{\sigma}^2 = \frac{b_n}{a_n - 1}$. Let $\theta = (\beta, \gamma, \sigma^2)^\top$, $W = \begin{bmatrix} X & I_n \end{bmatrix}$. Then, $\text{DIC}(\rho) = -2 \log p(y|\hat{\theta}) + 2p_{\text{DIC}}$ where

$$\begin{aligned} \log p(y|\theta) &= -\frac{n}{2} \log(2\pi(1-\rho)) - \frac{n}{2} \log(\sigma^2) - \frac{(y - W\gamma_\star)^\top (y - W\gamma_\star)}{2\sigma^2(1-\rho)} \\ \log p(y|\hat{\theta}) &= -\frac{n}{2} \log(2\pi(1-\rho)) - \frac{n}{2} \log\left(\frac{b_n}{a_n - 1}\right) - \frac{(a_n - 1) \|y - WM_\star m_\star\|^2}{2b_1(1-\rho)} \\ \mathbb{E}_{\theta|y} [\log p(y|\theta)] &= -\frac{n}{2} \log(2\pi(1-\rho)) + \frac{n}{2} (\psi(a_n) - \log(b_n)) - \frac{\text{tr}(WM_\star W^\top)}{2(1-\rho)} - \frac{a_n \|y - WM_\star m_\star\|^2}{2b_1(1-\rho)} \\ p_{\text{DIC}} &= \frac{n}{2} (\log(a_n - 1) - \psi(a_n)) + \frac{\text{tr}(WM_\star W^\top)}{2(1-\rho)} + \frac{\|y - WM_\star m_\star\|^2}{2b_1(1-\rho)} \end{aligned}$$

where $\psi(\cdot)$ is the digamma function. We now show that $\lim_{\rho \rightarrow 1^-} b_n(\rho) < \infty$. Denote $B = \frac{1-\rho}{\rho} V_\phi^{-1} + I_n - H$. Then, simplifications reveal $b_n = b_{\sigma^2} + \frac{1}{2(1-\rho)} (y^\top y - y^\top X \hat{\beta} - y^\top (I_n - H) \hat{\gamma})$, where $\hat{\gamma} = B^{-1}(I_n - H)y$. An alternative expression is $b_n = b_{\sigma^2} + \frac{1}{2(1-\rho)} e^\top (I - B^{-1})e$. By spectral decomposition, $V_\phi^{1/2}(I - H)V_\phi^{1/2} = CDC^\top$ where C is an orthogonal matrix and $D = \text{diag}(d_1, \dots, d_n)$ with entries that are the non-negative eigenvalues of $V_\phi^{1/2}(I - H)V_\phi^{1/2}$. Let $U = V_\phi^{1/2}C$, then U is invertible, $U^\top V_\phi^{-1}U = I_n$, $U^\top (I_n - H)U = D$, and $B^{-1} = U \left(D + \frac{1-\rho}{\rho} I_n \right)^{-1} U^\top$.

Define $v = U^{-1}e$, then $e^T B^{-1}e = v^T D \left(D + \frac{1-\rho}{\rho} I_n \right)^{-1} Dv$ and

$$\begin{aligned}
\lim_{\rho \rightarrow 1^-} b_n &= \lim_{\rho \rightarrow 1^-} b_{\sigma^2} + \frac{1}{2(1-\rho)} e^T (I - B^{-1})e \\
&= b_{\sigma^2} + \lim_{\rho \rightarrow 1^-} \frac{1}{2(1-\rho)} \left(v^T Dv - v^T D \left(D + \frac{1-\rho}{\rho} I_n \right)^{-1} Dv \right) \\
&= b_{\sigma^2} + \lim_{\rho \rightarrow 1^-} \frac{\sum_{d_j \neq 0} \left(v_j^2 d_j - \frac{v_j^2 d_j^2}{d_j + \frac{1-\rho}{\rho}} \right)}{2(1-\rho)} \\
&= b_{\sigma^2} + \lim_{\rho \rightarrow 1^-} \sum_{d_j \neq 0} \left(\frac{v_j^2 d_j^2}{2\rho^2 \left(d_j + \frac{1-\rho}{\rho} \right)^2} \right) = b_{\sigma^2} + \sum_{d_j \neq 0} \frac{v_j^2}{2} < \infty
\end{aligned}$$

where the second to last equality follows from L'Hôpital's Rule. Denote $b = \lim_{\rho \rightarrow 1^-} b_n(\rho) = b_{\sigma^2} + \sum_{d_j \neq 0} v_j^2/2$. We now show $\lim_{\rho \rightarrow 1^-} \frac{\|y - WM_{\star} m_{\star}\|^2}{1-\rho} = 0$. Expanding terms shows $y - W\hat{\gamma}_{\star} = (I_n - H)(I - B^{-1})e$ where $H = X(X^T X)^{-1} X^T$. Furthermore, $\|y - WM_{\star} m_{\star}\|^2 = e^T (I_n - H - 2B^{-1} + B^{-1}(I_n - H)B^{-1})e = v^T \left(D - 2D^2 \left[D + \frac{1-\rho}{\rho} I_n \right]^{-1} + D^3 \left[D + \frac{1-\rho}{\rho} I_n \right]^{-2} \right) v$ and

$$\begin{aligned}
\lim_{\rho \rightarrow 1^-} \frac{\|y - WM_{\star} m_{\star}\|^2}{1-\rho} &= \lim_{\rho \rightarrow 1^-} \sum_{d_j \neq 0} \frac{v_j^2}{1-\rho} \left(d_j - 2 \frac{d_j^2}{d_j + \frac{1-\rho}{\rho}} + \frac{d_j^3}{\left(d_j + \frac{1-\rho}{\rho} \right)^2} \right) \\
&= - \lim_{\rho \rightarrow 1^-} \sum_{d_j \neq 0} v_j^2 \left(-2 \frac{d_j^2}{\left(d_j + \frac{1-\rho}{\rho} \right)^2 \rho^2} + \frac{2d_j^3}{\left(d_j + \frac{1-\rho}{\rho} \right)^3 \rho^2} \right)
\end{aligned}$$

which can be evaluated to give the result $\lim_{\rho \rightarrow 1^-} \frac{\|y - WM_{\star} m_{\star}\|^2}{1-\rho} = 0$. Next, evaluating the expression $\frac{W^T W M_{\star}}{1-\rho}$ yields $\frac{\text{tr}(W M_{\star} W^T)}{1-\rho} = p + \text{tr}((I_n - H)B^{-1})$. Furthermore,

$$\begin{aligned}
\lim_{\rho \rightarrow 1^-} \text{tr} \left((I_n - H)B^{-1} \right) &= \lim_{\rho \rightarrow 1^-} \text{tr} \left((I_n - H)U \left(D + \frac{1-\rho}{\rho} I_n \right)^{-1} U^T \right) \\
&= \lim_{\rho \rightarrow 1^-} \text{tr} \left(D \left(D + \frac{1-\rho}{\rho} I_n \right)^{-1} \right) \\
&= \lim_{\rho \rightarrow 1^-} \sum_{d_j \neq 0} \frac{d_j}{d_j + \frac{1-\rho}{\rho}} \\
&= \sum_{d_j \neq 0} 1 = \text{tr}(I_n - H) = n - p
\end{aligned}$$

Therefore, $\lim_{\rho \rightarrow 1^-} \frac{\text{tr}(WM_\star W^T)}{1-\rho} = n$. Combining our previous results, we have shown that

$$\lim_{\rho \rightarrow 1^-} p_{DIC} = \lim_{\rho \rightarrow 1^-} 2 \left(\log p(y|\hat{\theta}) - \mathbb{E}_{\theta|y} [\log p(y|\theta)] \right) = n + n(\log(a_n - 1) - \psi(a_n))$$

p_{DIC} represents the number of effective parameters in the model and if n is large enough, a_{σ^2} small enough, then $\lim_{\rho \rightarrow 1^-} p_{DIC} \approx n+1$, which penalises heavy overfitting through the n spatial residuals. We have also shown that every term in $\log p(y|\hat{\theta})$ converges except $-\frac{n}{2} \log(2\pi(1-\rho))$, which diverges to ∞ as ρ becomes arbitrarily close to 1. Therefore, this shows that $\lim_{\rho \rightarrow 1^-} \text{DIC}(\rho) = \lim_{\rho \rightarrow 1^-} (-2 \log p(y|\hat{\theta}) + 2p_{DIC}) = -\infty$.

S5. BEHAVIOR OF WAIC IN SELECTING ρ IN EXACT MODEL

We sketch out an argument for the behaviour of WAIC as ρ grows arbitrarily close to 1 in the exact model. As for the DIC, we can show that $\lim_{\rho \rightarrow 1^-} p_{WAIC2} < \infty$, so it suffices to show that $\lim_{\rho \rightarrow 1^-} \text{lppd}(\rho) = \sum_{i=1}^n \lim_{\rho \rightarrow 1^-} \log(p_{\text{post}}(y_i)) = \infty$.

We consider the model given by (1), where the prior is $\pi(\beta, \gamma, \sigma^2) = N(\gamma | 0, \sigma^2 \rho V_\phi) \times \text{IG}(\sigma^2 | a_{\sigma^2}, b_{\sigma^2})$ and the modeled response $Y | \beta, \gamma, \sigma^2, \rho \sim N(X\beta + \gamma, \sigma^2(1-\rho))$ where we assume $0 \leq \rho \leq 1$ and V_ϕ is positive definite are known. Let $W = \begin{bmatrix} X & I_n \end{bmatrix}$, then

$$\begin{aligned} p_{\text{post}}(Y | \sigma^2, \rho) &\propto \int_{\gamma_\star} \exp \left(-\frac{(Y - W\gamma_\star)^T (Y - W\gamma_\star)}{2\sigma^2(1-\rho)} - \frac{(\gamma_\star - M_\star m_\star)^T M_\star^{-1} (\gamma_\star - M_\star m_\star)}{2\sigma^2} \right) d\gamma_\star \\ &\propto \exp \left(-\frac{Y^T Y}{2\sigma^2(1-\rho)} - \frac{\left(\frac{1}{1-\rho} W^T Y + m_\star \right)^T \left(\frac{W^T W}{1-\rho} + M_\star^{-1} \right)^{-1} \left(\frac{1}{1-\rho} W^T Y + m_\star \right)}{2\sigma^2} \right) \end{aligned}$$

Let $V_1 = W^T W + (1-\rho)M_\star^{-1} = \begin{bmatrix} 2X^T X & 2X^T \\ 2X & 2I_n + \frac{1-\rho}{\rho} V_\phi^{-1} \end{bmatrix}$, then since $m_\star = \frac{1}{1-\rho} W^T y$, this simplifies to

$$\begin{aligned} p_{\text{post}}(Y | \sigma^2, \rho) &\propto \exp \left(\frac{Y^T Y - (Y + y)^T W V_1^{-1} W^T (Y + y)}{2\sigma^2(1-\rho)} \right) \\ &\propto \exp \left(\frac{Y^T (I_n - W V_1^{-1} W^T) Y - 2Y^T W V_1^{-1} W^T y}{2\sigma^2(1-\rho)} \right) \end{aligned}$$

Hence, $Y | y, \sigma^2, \rho \sim N_n \left((I_n - W V_1^{-1} W^T)^{-1} W V_1^{-1} W^T y, \sigma^2(1-\rho) (I_n - W V_1^{-1} W^T)^{-1} \right)$. Denoting $H = X(X^T X)^{-1} X^T$, $B = (I_n - H) + \frac{1-\rho}{\rho} V_\phi^{-1}$, we have $W V_1^{-1} W^T = \frac{1}{2} H + (I_n - H)(B + I_n - H)^{-1}(I_n - H)$. Let U, D be defined as in Section 2.2 such that $U^T V_\phi^{-1} U = I_n$, $U^T (I_n - H) U = D$, and $B^{-1} =$

$U \left(D + \frac{1-\rho}{\rho} I_n \right)^{-1} U^\top$. Then,

$$\begin{aligned} I_n - WV_1^{-1}W^\top &= I_n - \frac{1}{2}H - (I_n - H)(B + I_n - H)^{-1}(I_n - H) \\ &= I_n - \frac{1}{2}H - U^{-\top}DU^{-1} \left(2U^{-\top}DU^{-1} + \frac{1-\rho}{\rho}U^{-\top}U^{-1} \right)^{-1} U^{-\top}DU^{-1} \\ &= I_n - \frac{1}{2}H - U^{-\top}D \left(2D + \frac{1-\rho}{\rho}I_n \right)^{-1} DU^{-1} \end{aligned}$$

Let $W = D \left(2D + \frac{1-\rho}{\rho}I_n \right)^{-1} D$, then $W_{ii} = \frac{d_i^2}{2d_i + \frac{1-\rho}{\rho}}$. If $d_j = 0$, then $W_{jj} = 0$. If $d_j > 0$, then $W_{jj} \rightarrow \frac{1}{2}d_j$ as $\rho \rightarrow 1^-$. Thus, $\lim_{\rho \rightarrow 1^-} W = \frac{1}{2}D$. Hence,

$$\lim_{\rho \rightarrow 1^-} (I - WV_1^{-1}W^\top) = I - \frac{1}{2}H - \frac{1}{2}U^{-\top}DU^{-1} = I - \frac{1}{2}H - \frac{1}{2}(I_n - H) = \frac{1}{2}I$$

which also implies $\lim_{\rho \rightarrow 1^-} (I_n - WV_1^{-1}W^\top)^{-1} WV_1^{-1}W^\top = I_n$. Define $Z = \frac{Y-y}{\sqrt{2\sigma^2(1-\rho)}} \Big| y, \sigma^2, \rho$ with probability density function $f_{\text{post}}(z)$. The above work implies that for all $z \in \mathbb{R}$, $\lim_{\rho \rightarrow 1^-} f_{\text{post}}(z) = f(z)$, where f denotes the standard normal CDF. As ρ goes arbitrarily close to 1, the modelled response $Y | y, \sigma^2, \rho$ converges in distribution to $N_n(y, 2\sigma^2(1-\rho)I_n)$. By this argument, $Y_i | y, \sigma^2, \rho$ converges in distribution to $N(y_i | 2\sigma^2(1-\rho))$ when $\rho \rightarrow 1^-$ for $i = 1, \dots, n$. Denote the pdf of $Y_i | y, \sigma^2, \rho$ as $f_{Y_i}(y_i | \sigma^2, \rho)$, then this directly implies that $\lim_{\rho \rightarrow 1^-} \log(p_{\text{post}}(y_i)) = \lim_{\rho \rightarrow 1^-} \int_0^\infty f_{Y_i}(y_i | \sigma^2, \rho) \pi(\sigma^2 | y, \rho) d\sigma^2 = \infty$. Hence, $\lim_{\rho \rightarrow 1^-} \text{lppd}(\rho) = \infty$, so $\text{WAIC}(\rho) = -2\text{lppd} + 2p_{\text{WAIC}2}$ diverges to $-\infty$ as $\rho \rightarrow 1^-$.

S6. CONSTRUCTION OF DIFFERENCE PROBABILITIES ON MODELLED RESPONSE LEVEL

Suppose the modelled response $Y | \beta, \gamma, \sigma^2, \rho \sim N(X\beta + \gamma, \sigma^2(1-\rho))$ and the prior is $\pi(\beta, \gamma, \sigma^2) = N(\gamma | 0, \sigma^2 \rho V_\phi) \times \text{IG}(\sigma^2 | a_{\sigma^2}, b_{\sigma^2})$. We begin with assuming $0 \leq \rho \leq 1$ and positive definite V_ϕ are known. Denote $\gamma_\star = (\beta^\top, \gamma^\top)^\top$.

Consider linear combinations of the modelled response $c_k^\top Y$ where $c_1, \dots, c_K \in \mathbb{R}^n$. Let $\gamma_\star = (\beta, \gamma)^\top$, and as discussed in Section 2.1, $\gamma_\star | \sigma^2, \rho \sim N(M_\star m_\star, \sigma^2 M_\star)$, $\sigma^2 | y, \rho \sim \text{IG}(a_n, b_n)$. Next, $Y | y, \sigma^2, \rho \sim N_n \left((I_n - WV_1^{-1}W^\top)^{-1} WV_1^{-1}W^\top y, \sigma^2(1-\rho) (I_n - WV_1^{-1}W^\top)^{-1} \right)$ as shown in Section S5, where $WV_1^{-1}W^\top = \frac{1}{2}H + (I_n - H)(B + I_n - H)^{-1}(I_n - H)$, $B = I_n - H + \frac{1-\rho}{\rho}V_\phi^{-1}$ and V_ϕ is assumed positive definite. For $\epsilon > 0$, define the conditional ϵ -difference probabilities as

$$h_k(\epsilon; \rho) = \mathbb{P} \left(\frac{|c_k^\top Y| / \sqrt{\sigma^2(1-\rho)}}{\sqrt{c_k^\top (I_n - WV_1^{-1}W^\top)^{-1} c_k}} > \epsilon \Big| y, \rho \right)$$

for $k = 1, \dots, K$. Let $0 \neq c_i, c_j \in \mathbb{R}^n$ and set $\alpha_i = \frac{\mathbb{E}(c_i^T Y | y, \sigma^2, \rho)}{\sqrt{\text{Var}(c_i^T Y | y, \sigma^2, \rho)}} = \frac{c_i^T (I_n - W V_1^{-1} W^T)^{-1} W V_1^{-1} y}{\sqrt{(1-\rho) c_i^T (I_n - W V_1^{-1} W^T)^{-1} c_i}}$. We show that the rankings of these posterior probabilities are stable by proving that given two vectors $c_i, c_j \in \mathbb{R}^n, 0 < \rho < 1$, if the corresponding conditional probabilities satisfy $h_i(\epsilon; \rho) < h_j(\epsilon; \rho)$ for some $\epsilon > 0$, then $h_i(\epsilon; \rho) < h_j(\epsilon; \rho)$ for all $\epsilon > 0$. First, define

$$\begin{aligned} w_i(\epsilon; \sigma^2, \rho) &= \mathbb{P} \left(\frac{|c_i^T Y| / \sqrt{\sigma^2(1-\rho)}}{\sqrt{c_i^T (I_n - W V_1^{-1} W^T)^{-1} c_i}} > \epsilon \mid y, \sigma^2, \rho \right) \\ &= \mathbb{P} \left(-\epsilon - \frac{\alpha_i}{\sigma} \leq Z \leq \epsilon - \frac{\alpha_i}{\sigma} \right), \quad Z \sim N(0, 1) \\ &= \Phi \left(-\epsilon + \frac{\alpha_i}{\sigma} \right) + \Phi \left(-\epsilon - \frac{\alpha_i}{\sigma} \right) \end{aligned}$$

where Φ denotes the standard normal CDF. Let $f : \mathbb{R} \rightarrow \mathbb{R}$ be given by $f(x) = \Phi(-\epsilon + \frac{x}{\sigma}) + \Phi(-\epsilon - \frac{x}{\sigma})$ for any $\sigma > 0$. Then, as shown in Proof of Theorem 1, for any $x, y \in \mathbb{R}, |x| > |y|$ if and only if $f(x) > f(y)$. Therefore, for any $\sigma^2 > 0$, $w_i(\epsilon; \sigma^2, \rho) > w_j(\epsilon; \sigma^2, \rho)$ if and only if $|\alpha_i(\sigma^2)| > |\alpha_j(\sigma^2)|$. Thus, if $|\alpha_i| > |\alpha_j|$, then

$$h_i(\epsilon; \rho) = \int_0^\infty w_i(\epsilon; \sigma^2, \rho) \pi(\sigma^2 | y) d\sigma^2 < \int_0^\infty w_j(\epsilon; \sigma^2, \rho) \pi(\sigma^2 | y) d\sigma^2 = h_j(\epsilon; \rho)$$

for all $\epsilon > 0$. Likewise, if $h_i(\epsilon; \rho) < h_j(\epsilon; \rho)$ for all ϵ , then there exists $\epsilon > 0, \sigma^2 > 0$ such that $w_i(\epsilon; \sigma^2, \rho) > w_j(\epsilon; \sigma^2, \rho)$ which implies $|\alpha_i| > |\alpha_j|$. Since the statement $|\alpha_i| > |\alpha_j|$ does not depend on ϵ , we conclude that if $h_i(\epsilon; \rho) < h_j(\epsilon; \rho)$ for some given $\epsilon > 0$, then $h_i(\epsilon; \rho) < h_j(\epsilon; \rho)$ for all $\epsilon > 0$.

Similar to the ϵ -difference probabilities on the effects level, one can define the corresponding marginal posterior ϵ -difference probabilities as

$$v_k(\epsilon) = \mathbb{P} \left(\frac{|c_k^T Y| / \sqrt{\sigma^2(1-\rho)}}{\sqrt{c_k^T (I_n - W V_1^{-1} W^T)^{-1} c_k}} > \epsilon \mid y \right).$$

S7. CLASSIFIED SPATIAL DISPARITIES IN COUNTY-LEVEL TRACHEAL, BRONCHUS, AND LUNG CANCER MORTALITY RATES

In Section 5, we apply the maximum conditional entropy criterion to select the difference threshold $\epsilon_{CE} = 0.845$ and set the Bayesian FDR tolerance at $\delta = 0.2$ to obtain 460 classified spatial difference boundaries out of 8,793 pairs of geographically adjacent counties within the continental USA. The full list of disparities are shown in Table S1, along with Monte Carlo estimates of $v_k(\epsilon_{CE}) = \mathbb{P} \left(\frac{|a_k^T \phi|}{\sqrt{a_k^T \text{Var}(\phi | y, \rho) a_k}} > \epsilon \mid y \right)$.

	County 1	County 2	$v_k(\epsilon_{CE})$
1	Alachua County, Florida	Union County, Florida	1.000
2	Baker County, Florida	Union County, Florida	1.000
3	Bradford County, Florida	Union County, Florida	1.000
4	Columbia County, Florida	Union County, Florida	1.000
5	Boone County, Kentucky	Gallatin County, Kentucky	1.000
6	Clark County, Kentucky	Powell County, Kentucky	1.000
7	Montgomery County, Kentucky	Powell County, Kentucky	1.000
8	Pike County, Kentucky	Buchanan County, Virginia	1.000
9	Attala County, Mississippi	Madison County, Mississippi	1.000
10	Hinds County, Mississippi	Madison County, Mississippi	1.000
11	Holmes County, Mississippi	Madison County, Mississippi	1.000
12	Leake County, Mississippi	Madison County, Mississippi	1.000
13	Lee County, Mississippi	Union County, Mississippi	1.000
14	Madison County, Mississippi	Rankin County, Mississippi	1.000
15	Madison County, Mississippi	Scott County, Mississippi	1.000
16	Madison County, Mississippi	Yazoo County, Mississippi	1.000
17	Pierce County, North Dakota	Rolette County, North Dakota	1.000
18	Guernsey County, Ohio	Noble County, Ohio	1.000
19	Muskingum County, Ohio	Noble County, Ohio	1.000
20	Noble County, Ohio	Washington County, Ohio	1.000
21	Chattahoochee County, Georgia	Marion County, Georgia	1.000
22	McCreary County, Kentucky	Wayne County, Kentucky	1.000
23	Menifee County, Kentucky	Powell County, Kentucky	1.000
24	Anson County, North Carolina	Marlboro County, South Carolina	1.000
25	Caldwell Parish, Louisiana	Franklin Parish, Louisiana	1.000
26	Switzerland County, Indiana	Gallatin County, Kentucky	1.000
27	Carroll County, Kentucky	Gallatin County, Kentucky	1.000
28	Robeson County, North Carolina	Marlboro County, South Carolina	1.000
29	Gallatin County, Kentucky	Owen County, Kentucky	1.000
30	Clay County, Kentucky	Perry County, Kentucky	1.000
31	Jackson County, Kentucky	Owsley County, Kentucky	1.000
32	Jeff Davis County, Georgia	Wheeler County, Georgia	1.000
33	Martin County, Kentucky	Wayne County, West Virginia	1.000
34	Bottineau County, North Dakota	Rolette County, North Dakota	1.000
35	Coshocton County, Ohio	Holmes County, Ohio	1.000
36	Lampasas County, Texas	San Saba County, Texas	1.000

37	Lee County, Mississippi	Pontotoc County, Mississippi	1.000
38	Frederick County, Virginia	Hardy County, West Virginia	1.000
39	Boone County, West Virginia	Raleigh County, West Virginia	1.000
40	Cumberland County, Tennessee	Fentress County, Tennessee	1.000
41	Buchanan County, Virginia	Mingo County, West Virginia	1.000
42	Rolette County, North Dakota	Towner County, North Dakota	0.999
43	Letcher County, Kentucky	Dickenson County, Virginia	0.999
44	Allen Parish, Louisiana	Vernon Parish, Louisiana	0.999
45	Madison County, Missouri	Perry County, Missouri	0.999
46	Bell County, Kentucky	Leslie County, Kentucky	0.999
47	Laurel County, Kentucky	McCreary County, Kentucky	0.999
48	Holmes County, Ohio	Knox County, Ohio	0.999
49	Johnson County, Kentucky	Morgan County, Kentucky	0.999
50	Pickett County, Tennessee	Scott County, Tennessee	0.999
51	Boyd County, Kentucky	Lawrence County, Kentucky	0.999
52	Richmond County, North Carolina	Marlboro County, South Carolina	0.999
53	Fulton County, Kentucky	Hickman County, Kentucky	0.999
54	Choctaw County, Mississippi	Webster County, Mississippi	0.999
55	Anderson County, Tennessee	Scott County, Tennessee	0.999
56	Issaquena County, Mississippi	Washington County, Mississippi	0.999
57	Gallatin County, Kentucky	Grant County, Kentucky	0.999
58	Hardin County, Illinois	Pope County, Illinois	0.999
59	Lincoln County, Tennessee	Moore County, Tennessee	0.999
60	Lampasas County, Texas	Mills County, Texas	0.998
61	Apache County, Arizona	Greenlee County, Arizona	0.998
62	Gilmer County, Georgia	Murray County, Georgia	0.998
63	Chesterfield County, South Carolina	Marlboro County, South Carolina	0.998
64	Dooly County, Georgia	Houston County, Georgia	0.998
65	Coffee County, Tennessee	Moore County, Tennessee	0.998
66	Chattahoochee County, Georgia	Webster County, Georgia	0.998
67	Clay County, Kentucky	Owsley County, Kentucky	0.998
68	Pendleton County, West Virginia	Pocahontas County, West Virginia	0.998
69	Florence County, South Carolina	Marlboro County, South Carolina	0.998
70	Bryan County, Georgia	Chatham County, Georgia	0.998
71	Knott County, Kentucky	Perry County, Kentucky	0.998
72	McCreary County, Kentucky	Pulaski County, Kentucky	0.998
73	Harlan County, Kentucky	Wise County, Virginia	0.998
74	Carter County, Missouri	Oregon County, Missouri	0.998

75	Caldwell Parish, Louisiana	Ouachita Parish, Louisiana	0.997
76	Monroe County, Ohio	Noble County, Ohio	0.997
77	East Carroll Parish, Louisiana	Issaquena County, Mississippi	0.997
78	Issaquena County, Mississippi	Sharkey County, Mississippi	0.997
79	Morgan County, Ohio	Noble County, Ohio	0.997
80	Morgan County, Tennessee	Scott County, Tennessee	0.997
81	Morgan County, Kentucky	Wolfe County, Kentucky	0.997
82	Jefferson County, Indiana	Scott County, Indiana	0.997
83	Ashland County, Ohio	Holmes County, Ohio	0.997
84	Anderson County, Texas	Cherokee County, Texas	0.997
85	Clark County, Indiana	Scott County, Indiana	0.997
86	Boone County, West Virginia	Kanawha County, West Virginia	0.997
87	Camden County, Missouri	Pulaski County, Missouri	0.997
88	Posey County, Indiana	Union County, Kentucky	0.997
89	La Paz County, Arizona	San Bernardino County, California	0.997
90	Haakon County, South Dakota	Ziebach County, South Dakota	0.997
91	Wayne County, Kentucky	Scott County, Tennessee	0.996
92	Sheridan County, Montana	Divide County, North Dakota	0.996
93	Craighead County, Arkansas	Poinsett County, Arkansas	0.996
94	Marion County, Florida	Sumter County, Florida	0.996
95	Lee County, Mississippi	Prentiss County, Mississippi	0.996
96	Scott County, Indiana	Washington County, Indiana	0.996
97	Bienville Parish, Louisiana	Red River Parish, Louisiana	0.996
98	Grand County, Utah	San Juan County, Utah	0.996
99	Belmont County, Ohio	Noble County, Ohio	0.995
100	Cherokee County, North Carolina	Polk County, Tennessee	0.995
101	Gallatin County, Illinois	Posey County, Indiana	0.995
102	Meriwether County, Georgia	Pike County, Georgia	0.995
103	Union County, Illinois	Perry County, Missouri	0.995
104	Carter County, Missouri	Reynolds County, Missouri	0.995
105	Benson County, North Dakota	Nelson County, North Dakota	0.995
106	Harlan County, Kentucky	Lee County, Virginia	0.995
107	Breathitt County, Kentucky	Magoffin County, Kentucky	0.995
108	Bullitt County, Kentucky	Hardin County, Kentucky	0.995
109	Pike County, Kentucky	Dickenson County, Virginia	0.995
110	Alexander County, Illinois	Cape Girardeau County, Missouri	0.995
111	Reynolds County, Missouri	Wayne County, Missouri	0.995
112	Estill County, Kentucky	Powell County, Kentucky	0.994

113	Lee County, Mississippi	Monroe County, Mississippi	0.994
114	Chicot County, Arkansas	Issaquena County, Mississippi	0.994
115	Clearwater County, Idaho	Shoshone County, Idaho	0.994
116	Plaquemines Parish, Louisiana	Saint Bernard Parish, Louisiana	0.994
117	Perry County, Missouri	Saint Francois County, Missouri	0.994
118	Scotland County, North Carolina	Marlboro County, South Carolina	0.994
119	Macon County, Georgia	Peach County, Georgia	0.994
120	Jeff Davis County, Georgia	Telfair County, Georgia	0.994
121	East Feliciana Parish, Louisiana	Amite County, Mississippi	0.994
122	Clinch County, Georgia	Echols County, Georgia	0.994
123	Bienville Parish, Louisiana	Claiborne Parish, Louisiana	0.994
124	Anderson County, Texas	Freestone County, Texas	0.994
125	Effingham County, Georgia	Jasper County, South Carolina	0.994
126	Arkansas County, Arkansas	Lincoln County, Arkansas	0.994
127	Jefferson County, Alabama	Walker County, Alabama	0.994
128	Magoffin County, Kentucky	Morgan County, Kentucky	0.994
129	Jackson County, Kentucky	Lee County, Kentucky	0.994
130	Lawrence County, Kentucky	Wayne County, West Virginia	0.994
131	Fannin County, Georgia	Polk County, Tennessee	0.993
132	Benton County, Missouri	Camden County, Missouri	0.993
133	Sumner County, Tennessee	Trousdale County, Tennessee	0.993
134	Burnet County, Texas	Lampasas County, Texas	0.993
135	Union County, Arkansas	Claiborne Parish, Louisiana	0.993
136	Jackson County, Indiana	Scott County, Indiana	0.993
137	Chickasaw County, Mississippi	Lee County, Mississippi	0.993
138	Anderson County, Texas	Houston County, Texas	0.993
139	Hickman County, Tennessee	Williamson County, Tennessee	0.992
140	Flagler County, Florida	Putnam County, Florida	0.992
141	Bleckley County, Georgia	Pulaski County, Georgia	0.992
142	Elliott County, Kentucky	Lawrence County, Kentucky	0.992
143	Blount County, Alabama	Walker County, Alabama	0.992
144	Coconino County, Arizona	Mohave County, Arizona	0.992
145	Pulaski County, Missouri	Texas County, Missouri	0.992
146	Burt County, Nebraska	Cuming County, Nebraska	0.992
147	La Paz County, Arizona	Mohave County, Arizona	0.992
148	Glades County, Florida	Okeechobee County, Florida	0.992
149	Franklin County, Illinois	Perry County, Illinois	0.992
150	Sierra County, California	Yuba County, California	0.991

151	McCreary County, Kentucky	Campbell County, Tennessee	0.991
152	Apache County, Arizona	Montezuma County, Colorado	0.991
153	Peach County, Georgia	Taylor County, Georgia	0.991
154	Bedford County, Tennessee	Moore County, Tennessee	0.991
155	Dooly County, Georgia	Sumter County, Georgia	0.991
156	Citrus County, Florida	Sumter County, Florida	0.991
157	Letcher County, Kentucky	Perry County, Kentucky	0.990
158	Cleburne County, Alabama	Randolph County, Alabama	0.990
159	Clay County, Kentucky	Leslie County, Kentucky	0.990
160	Breathitt County, Kentucky	Wolfe County, Kentucky	0.990
161	Haywood County, North Carolina	Cocke County, Tennessee	0.990
162	Issaquena County, Mississippi	Yazoo County, Mississippi	0.990
163	Montgomery County, Georgia	Wheeler County, Georgia	0.990
164	Bradley County, Tennessee	Polk County, Tennessee	0.990
165	Mesa County, Colorado	San Juan County, Utah	0.989
166	Randolph County, West Virginia	Webster County, West Virginia	0.989
167	Hernando County, Florida	Sumter County, Florida	0.989
168	Dewey County, Oklahoma	Major County, Oklahoma	0.989
169	Iron County, Missouri	Reynolds County, Missouri	0.989
170	Breathitt County, Kentucky	Knott County, Kentucky	0.989
171	Dewey County, South Dakota	Ziebach County, South Dakota	0.989
172	Bell County, Kentucky	Harlan County, Kentucky	0.989
173	Pasco County, Florida	Sumter County, Florida	0.989
174	Dade County, Georgia	Hamilton County, Tennessee	0.989
175	Grenada County, Mississippi	Montgomery County, Mississippi	0.989
176	La Paz County, Arizona	Riverside County, California	0.989
177	Dubois County, Indiana	Orange County, Indiana	0.989
178	Cedar County, Nebraska	Clay County, South Dakota	0.988
179	Apache County, Arizona	Graham County, Arizona	0.988
180	Franklin County, Kentucky	Shelby County, Kentucky	0.988
181	Lincoln County, West Virginia	Putnam County, West Virginia	0.988
182	Clinton County, Missouri	DeKalb County, Missouri	0.987
183	Chase County, Kansas	Marion County, Kansas	0.987
184	Carroll County, Mississippi	Grenada County, Mississippi	0.987
185	Desha County, Arkansas	Coahoma County, Mississippi	0.986
186	Ben Hill County, Georgia	Wilcox County, Georgia	0.986
187	Gilmer County, Georgia	Gordon County, Georgia	0.986
188	Mingo County, West Virginia	Wayne County, West Virginia	0.986

189	Spencer County, Indiana	Daviess County, Kentucky	0.986
190	Laurel County, Kentucky	Whitley County, Kentucky	0.985
191	Hardin County, Illinois	Livingston County, Kentucky	0.985
192	Bullock County, Alabama	Russell County, Alabama	0.985
193	Baker County, Georgia	Decatur County, Georgia	0.985
194	Dent County, Missouri	Iron County, Missouri	0.985
195	Bent County, Colorado	Prowers County, Colorado	0.984
196	Darlington County, South Carolina	Marlboro County, South Carolina	0.984
197	Meade County, South Dakota	Ziebach County, South Dakota	0.984
198	Clark County, Kentucky	Estill County, Kentucky	0.984
199	Harrison County, Iowa	Shelby County, Iowa	0.984
200	Brown County, Illinois	Cass County, Illinois	0.984
201	Dooly County, Georgia	Macon County, Georgia	0.984
202	Franklin County, Tennessee	Moore County, Tennessee	0.984
203	Alcorn County, Mississippi	Tippah County, Mississippi	0.983
204	Allen Parish, Louisiana	Beauregard Parish, Louisiana	0.983
205	Cheatham County, Tennessee	Williamson County, Tennessee	0.983
206	Caldwell Parish, Louisiana	Richland Parish, Louisiana	0.983
207	Davis County, Iowa	Monroe County, Iowa	0.983
208	Shenandoah County, Virginia	Hardy County, West Virginia	0.983
209	Tallahatchie County, Mississippi	Yalobusha County, Mississippi	0.982
210	Marion County, Kentucky	Washington County, Kentucky	0.982
211	Pottawattamie County, Iowa	Shelby County, Iowa	0.982
212	Desha County, Arkansas	Phillips County, Arkansas	0.981
213	Dyer County, Tennessee	Lake County, Tennessee	0.981
214	Holmes County, Ohio	Wayne County, Ohio	0.980
215	Chambers County, Alabama	Randolph County, Alabama	0.980
216	Banks County, Georgia	Jackson County, Georgia	0.979
217	Richmond County, Georgia	Edgefield County, South Carolina	0.979
218	Grainger County, Tennessee	Jefferson County, Tennessee	0.979
219	Live Oak County, Texas	San Patricio County, Texas	0.979
220	Levy County, Florida	Marion County, Florida	0.978
221	Jefferson County, Texas	Liberty County, Texas	0.978
222	Crawford County, Iowa	Harrison County, Iowa	0.977
223	Clay County, Kansas	Geary County, Kansas	0.977
224	Adams County, Wisconsin	Wood County, Wisconsin	0.977
225	Adams County, Indiana	Jay County, Indiana	0.977
226	Tuscaloosa County, Alabama	Walker County, Alabama	0.977

227	Coffee County, Georgia	Jeff Davis County, Georgia	0.977
228	Kemper County, Mississippi	Newton County, Mississippi	0.977
229	Nemaha County, Kansas	Pottawatomie County, Kansas	0.977
230	Hamilton County, Texas	Lampasas County, Texas	0.976
231	Carter County, Montana	Custer County, Montana	0.976
232	Bracken County, Kentucky	Harrison County, Kentucky	0.976
233	Mercer County, Kentucky	Washington County, Kentucky	0.976
234	Citrus County, Florida	Levy County, Florida	0.976
235	Sheridan County, Montana	Williams County, North Dakota	0.975
236	Dillon County, South Carolina	Marlboro County, South Carolina	0.975
237	Barbour County, Alabama	Bullock County, Alabama	0.975
238	McDuffie County, Georgia	Taliaferro County, Georgia	0.975
239	Craighead County, Arkansas	Dunklin County, Missouri	0.975
240	Grant County, Indiana	Wells County, Indiana	0.975
241	Jennings County, Indiana	Scott County, Indiana	0.975
242	Bee County, Texas	Refugio County, Texas	0.975
243	Bacon County, Georgia	Coffee County, Georgia	0.975
244	McKinley County, New Mexico	Sandoval County, New Mexico	0.974
245	Crowley County, Colorado	Kiowa County, Colorado	0.974
246	Leake County, Mississippi	Neshoba County, Mississippi	0.974
247	Hickman County, Kentucky	Mississippi County, Missouri	0.973
248	Allen Parish, Louisiana	Jefferson Davis Parish, Louisiana	0.973
249	LaGrange County, Indiana	Saint Joseph County, Michigan	0.973
250	Comanche County, Kansas	Woods County, Oklahoma	0.973
251	Franklin County, Tennessee	Marion County, Tennessee	0.972
252	Trousdale County, Tennessee	Wilson County, Tennessee	0.972
253	Chester County, Tennessee	McNairy County, Tennessee	0.972
254	Nye County, Nevada	White Pine County, Nevada	0.971
255	Pope County, Illinois	Saline County, Illinois	0.971
256	Wibaux County, Montana	Golden Valley County, North Dakota	0.971
257	Caldwell Parish, Louisiana	Catahoula Parish, Louisiana	0.971
258	Macon County, Tennessee	Sumner County, Tennessee	0.970
259	Baker County, Florida	Charlton County, Georgia	0.970
260	Marion County, Georgia	Talbot County, Georgia	0.970
261	Charles County, Maryland	Prince George's County, Maryland	0.970
262	Camas County, Idaho	Elmore County, Idaho	0.969
263	Powell County, Kentucky	Wolfe County, Kentucky	0.969
264	Columbia County, Arkansas	Claiborne Parish, Louisiana	0.969

265	Loving County, Texas	Reeves County, Texas	0.969
266	Greene County, Arkansas	Dunklin County, Missouri	0.969
267	Crawford County, Indiana	Dubois County, Indiana	0.969
268	Russell County, Virginia	Wise County, Virginia	0.969
269	Bullock County, Alabama	Pike County, Alabama	0.969
270	Fallon County, Montana	Golden Valley County, North Dakota	0.968
271	Frederick County, Virginia	Hampshire County, West Virginia	0.968
272	Walker County, Georgia	Hamilton County, Tennessee	0.968
273	Clinch County, Georgia	Ware County, Georgia	0.968
274	Dooly County, Georgia	Wilcox County, Georgia	0.968
275	White County, Illinois	Gibson County, Indiana	0.968
276	Jackson County, Alabama	Franklin County, Tennessee	0.967
277	Angelina County, Texas	Polk County, Texas	0.967
278	Corson County, South Dakota	Dewey County, South Dakota	0.967
279	Cullman County, Alabama	Walker County, Alabama	0.967
280	Gloucester County, Virginia	Mathews County, Virginia	0.966
281	Calhoun County, Mississippi	Yalobusha County, Mississippi	0.966
282	Cassia County, Idaho	Elko County, Nevada	0.966
283	Alachua County, Florida	Marion County, Florida	0.966
284	Houston County, Georgia	Peach County, Georgia	0.966
285	Crisp County, Georgia	Dooly County, Georgia	0.966
286	Athens County, Ohio	Morgan County, Ohio	0.966
287	Douglas County, Missouri	Howell County, Missouri	0.965
288	Bee County, Texas	San Patricio County, Texas	0.965
289	Carter County, Kentucky	Lawrence County, Kentucky	0.965
290	Green County, Kentucky	Hart County, Kentucky	0.965
291	Liberty County, Montana	Pondera County, Montana	0.964
292	Estill County, Kentucky	Lee County, Kentucky	0.964
293	Nevada County, California	Yuba County, California	0.964
294	Guernsey County, Ohio	Tuscarawas County, Ohio	0.964
295	Dodge County, Georgia	Pulaski County, Georgia	0.964
296	Butts County, Georgia	Monroe County, Georgia	0.964
297	Butler County, Kansas	Marion County, Kansas	0.963
298	Clay County, Mississippi	Webster County, Mississippi	0.963
299	Madison County, North Carolina	Cocke County, Tennessee	0.963
300	Montgomery County, Mississippi	Webster County, Mississippi	0.963
301	Crockett County, Tennessee	Dyer County, Tennessee	0.963
302	Bledsoe County, Tennessee	Rhea County, Tennessee	0.962

303	Carroll County, Tennessee	Madison County, Tennessee	0.962
304	Menominee County, Wisconsin	Shawano County, Wisconsin	0.962
305	Van Buren County, Tennessee	Warren County, Tennessee	0.962
306	Roger Mills County, Oklahoma	Wheeler County, Texas	0.961
307	Jackson County, Arkansas	Poinsett County, Arkansas	0.961
308	Catoosa County, Georgia	Walker County, Georgia	0.961
309	Cecil County, Maryland	Lancaster County, Pennsylvania	0.961
310	Montgomery County, Arkansas	Yell County, Arkansas	0.960
311	Lee County, Arkansas	Monroe County, Arkansas	0.960
312	Fallon County, Montana	Slope County, North Dakota	0.960
313	Howard County, Arkansas	Montgomery County, Arkansas	0.960
314	Putnam County, Florida	Volusia County, Florida	0.960
315	Lake County, Tennessee	Obion County, Tennessee	0.960
316	Chester County, Tennessee	Henderson County, Tennessee	0.959
317	Bryan County, Georgia	Evans County, Georgia	0.959
318	Crockett County, Tennessee	Gibson County, Tennessee	0.959
319	Barry County, Missouri	McDonald County, Missouri	0.958
320	Bastrop County, Texas	Fayette County, Texas	0.958
321	Boyle County, Kentucky	Washington County, Kentucky	0.958
322	Crawford County, Missouri	Iron County, Missouri	0.958
323	Jefferson County, Montana	Madison County, Montana	0.958
324	Fannin County, Georgia	Murray County, Georgia	0.958
325	Preston County, West Virginia	Taylor County, West Virginia	0.957
326	Madison County, North Carolina	Greene County, Tennessee	0.957
327	Drew County, Arkansas	Lincoln County, Arkansas	0.957
328	Union County, Illinois	Cape Girardeau County, Missouri	0.957
329	Clay County, Georgia	Quitman County, Georgia	0.957
330	Cape Girardeau County, Missouri	Scott County, Missouri	0.957
331	Clinton County, Pennsylvania	Union County, Pennsylvania	0.957
332	McDowell County, West Virginia	Mercer County, West Virginia	0.957
333	Franklin County, Alabama	Marion County, Alabama	0.956
334	Kootenai County, Idaho	Shoshone County, Idaho	0.956
335	LaGrange County, Indiana	Noble County, Indiana	0.956
336	Polk County, Texas	Tyler County, Texas	0.956
337	Letcher County, Kentucky	Wise County, Virginia	0.956
338	Lawrence County, Kentucky	Morgan County, Kentucky	0.956
339	Decatur County, Indiana	Jennings County, Indiana	0.956
340	Hamilton County, Tennessee	Marion County, Tennessee	0.955

341	Van Buren County, Tennessee	White County, Tennessee	0.955
342	Lafayette County, Arkansas	Caddo Parish, Louisiana	0.955
343	Jackson County, Georgia	Oconee County, Georgia	0.955
344	Holmes County, Ohio	Tuscarawas County, Ohio	0.955
345	Claiborne Parish, Louisiana	Webster Parish, Louisiana	0.955
346	Monroe County, Arkansas	Saint Francis County, Arkansas	0.955
347	Harris County, Texas	Liberty County, Texas	0.955
348	Page County, Virginia	Warren County, Virginia	0.955
349	Daniels County, Montana	Valley County, Montana	0.955
350	Marion County, Alabama	Walker County, Alabama	0.954
351	Crawford County, Georgia	Peach County, Georgia	0.954
352	Garrard County, Kentucky	Rockcastle County, Kentucky	0.954
353	Grenada County, Mississippi	Tallahatchie County, Mississippi	0.954
354	Paulding County, Georgia	Polk County, Georgia	0.953
355	Blaine County, Idaho	Elmore County, Idaho	0.953
356	Houston County, Georgia	Pulaski County, Georgia	0.953
357	Brown County, Indiana	Jackson County, Indiana	0.953
358	Cabell County, West Virginia	Lincoln County, West Virginia	0.953
359	Marshall County, Kansas	Pottawatomie County, Kansas	0.953
360	Banks County, Georgia	Madison County, Georgia	0.953
361	Claiborne County, Tennessee	Hancock County, Tennessee	0.953
362	Jefferson County, Oregon	Linn County, Oregon	0.953
363	Lee County, Virginia	Scott County, Virginia	0.952
364	Hardin County, Illinois	Crittenden County, Kentucky	0.952
365	Chattahoochee County, Georgia	Muscogee County, Georgia	0.952
366	Grant County, West Virginia	Mineral County, West Virginia	0.952
367	Bryan County, Georgia	Bulloch County, Georgia	0.952
368	Buchanan County, Missouri	DeKalb County, Missouri	0.952
369	Delaware County, Oklahoma	Ottawa County, Oklahoma	0.951
370	Carroll County, Mississippi	Holmes County, Mississippi	0.951
371	Grant County, Kentucky	Harrison County, Kentucky	0.951
372	Shoshone County, Idaho	Sanders County, Montana	0.950
373	Duplin County, North Carolina	Onslow County, North Carolina	0.950
374	Cibola County, New Mexico	McKinley County, New Mexico	0.950
375	Coleman County, Texas	Concho County, Texas	0.950
376	Adair County, Kentucky	Casey County, Kentucky	0.950
377	Lincoln County, Nevada	Millard County, Utah	0.950
378	Atoka County, Oklahoma	Choctaw County, Oklahoma	0.949

379	Coahoma County, Mississippi	Tallahatchie County, Mississippi	0.949
380	Winnebago County, Illinois	Green County, Wisconsin	0.949
381	Clay County, West Virginia	Roane County, West Virginia	0.949
382	Callahan County, Texas	Jones County, Texas	0.949
383	Boundary County, Idaho	Lincoln County, Montana	0.949
384	Attala County, Mississippi	Choctaw County, Mississippi	0.949
385	Mono County, California	Lyon County, Nevada	0.949
386	Menifee County, Kentucky	Wolfe County, Kentucky	0.948
387	Atoka County, Oklahoma	Pushmataha County, Oklahoma	0.948
388	Worcester County, Maryland	Accomack County, Virginia	0.948
389	Juniata County, Pennsylvania	Perry County, Pennsylvania	0.948
390	Latah County, Idaho	Shoshone County, Idaho	0.948
391	Briscoe County, Texas	Donley County, Texas	0.947
392	Adams County, Ohio	Highland County, Ohio	0.947
393	Toombs County, Georgia	Treutlen County, Georgia	0.947
394	Lafayette County, Mississippi	Union County, Mississippi	0.947
395	Barbour County, West Virginia	Harrison County, West Virginia	0.947
396	Orleans Parish, Louisiana	Saint Bernard Parish, Louisiana	0.947
397	Highlands County, Florida	Okeechobee County, Florida	0.947
398	Jackson County, Illinois	Randolph County, Illinois	0.947
399	Bonner County, Idaho	Shoshone County, Idaho	0.946
400	Mesa County, Colorado	Pitkin County, Colorado	0.946
401	Fayette County, Tennessee	Tipton County, Tennessee	0.946
402	Montrose County, Colorado	San Juan County, Utah	0.946
403	Wayne County, Indiana	Darke County, Ohio	0.946
404	Cleveland County, Arkansas	Lincoln County, Arkansas	0.946
405	Bowman County, North Dakota	Slope County, North Dakota	0.946
406	McIntosh County, Georgia	Wayne County, Georgia	0.946
407	Buchanan County, Virginia	McDowell County, West Virginia	0.945
408	Hickman County, Kentucky	Obion County, Tennessee	0.945
409	Sioux County, Nebraska	Fall River County, South Dakota	0.945
410	Meriwether County, Georgia	Talbot County, Georgia	0.944
411	Rapides Parish, Louisiana	Vernon Parish, Louisiana	0.944
412	Franklin County, Missouri	Washington County, Missouri	0.944
413	Raleigh County, West Virginia	Wyoming County, West Virginia	0.944
414	Barrow County, Georgia	Gwinnett County, Georgia	0.944
415	Adams County, Indiana	Allen County, Indiana	0.944
416	Clay County, Kentucky	Laurel County, Kentucky	0.944

417	Benton County, Missouri	Hickory County, Missouri	0.944
418	Lake County, Florida	Sumter County, Florida	0.944
419	Benson County, North Dakota	Towner County, North Dakota	0.944
420	Scott County, Virginia	Wise County, Virginia	0.944
421	Dillon County, South Carolina	Horry County, South Carolina	0.944
422	Kanawha County, West Virginia	Lincoln County, West Virginia	0.943
423	Henry County, Kentucky	Shelby County, Kentucky	0.943
424	Howell County, Missouri	Texas County, Missouri	0.943
425	Eddy County, New Mexico	Loving County, Texas	0.943
426	Crittenden County, Arkansas	Shelby County, Tennessee	0.942
427	Murray County, Georgia	Bradley County, Tennessee	0.942
428	Ben Hill County, Georgia	Turner County, Georgia	0.942
429	Churchill County, Nevada	Pershing County, Nevada	0.941
430	Leake County, Mississippi	Winston County, Mississippi	0.941
431	Bollinger County, Missouri	Madison County, Missouri	0.941
432	Brown County, Illinois	Schuyler County, Illinois	0.941
433	Grant County, West Virginia	Randolph County, West Virginia	0.941
434	Oldham County, Kentucky	Trimble County, Kentucky	0.941
435	Fentress County, Tennessee	Pickett County, Tennessee	0.941
436	DeKalb County, Alabama	Dade County, Georgia	0.940
437	Bledsoe County, Tennessee	White County, Tennessee	0.940
438	Liberty County, Georgia	McIntosh County, Georgia	0.940
439	Cooper County, Missouri	Pettis County, Missouri	0.940
440	Sioux County, Iowa	Union County, South Dakota	0.940
441	Chattahoochee County, Georgia	Talbot County, Georgia	0.939
442	Monroe County, Illinois	Jefferson County, Missouri	0.939
443	Appanoose County, Iowa	Monroe County, Iowa	0.939
444	Wallowa County, Oregon	Columbia County, Washington	0.939
445	Long County, Georgia	McIntosh County, Georgia	0.939
446	Rusk County, Wisconsin	Taylor County, Wisconsin	0.938
447	Grant Parish, Louisiana	Rapides Parish, Louisiana	0.938
448	Henderson County, Kentucky	McLean County, Kentucky	0.938
449	Dewey County, Oklahoma	Woodward County, Oklahoma	0.938
450	Big Horn County, Montana	Treasure County, Montana	0.938
451	Elk County, Kansas	Wilson County, Kansas	0.938
452	Caldwell Parish, Louisiana	Winn Parish, Louisiana	0.938
453	Monroe County, Tennessee	Polk County, Tennessee	0.938
454	Hartley County, Texas	Sherman County, Texas	0.937

455	Monroe County, Iowa	Wayne County, Iowa	0.937
456	Grant County, West Virginia	Hampshire County, West Virginia	0.937
457	Cass County, Missouri	Henry County, Missouri	0.937
458	Overton County, Tennessee	Pickett County, Tennessee	0.937
459	Oktibbeha County, Mississippi	Webster County, Mississippi	0.936
460	Laclede County, Missouri	Pulaski County, Missouri	0.936
461	Pennington County, South Dakota	Ziebach County, South Dakota	0.936
462	Liberty County, Montana	Toole County, Montana	0.936
463	Gallatin County, Montana	Jefferson County, Montana	0.936
464	Bland County, Virginia	Smyth County, Virginia	0.935
465	Caldwell County, Missouri	DeKalb County, Missouri	0.935
466	Sequatchie County, Tennessee	Van Buren County, Tennessee	0.935
467	Price County, Wisconsin	Taylor County, Wisconsin	0.935
468	Shannon County, Missouri	Texas County, Missouri	0.934
469	Richmond County, Virginia	Westmoreland County, Virginia	0.934
470	Pope County, Arkansas	Van Buren County, Arkansas	0.934
471	Surry County, North Carolina	Patrick County, Virginia	0.933
472	Miller County, Missouri	Osage County, Missouri	0.933
473	Jones County, Texas	Shackelford County, Texas	0.933
474	George County, Mississippi	Greene County, Mississippi	0.933
475	Fleming County, Kentucky	Mason County, Kentucky	0.932
476	Delaware County, Iowa	Dubuque County, Iowa	0.932
477	Garrard County, Kentucky	Lincoln County, Kentucky	0.932
478	Cumberland County, Tennessee	Putnam County, Tennessee	0.932
479	Hall County, Georgia	Jackson County, Georgia	0.932
480	Custer County, Montana	Garfield County, Montana	0.932
481	Spencer County, Indiana	Hancock County, Kentucky	0.931
482	Issaquena County, Mississippi	Warren County, Mississippi	0.931
483	Roosevelt County, Montana	Sheridan County, Montana	0.931
484	Green County, Kentucky	Metcalf County, Kentucky	0.931
485	Bracken County, Kentucky	Clermont County, Ohio	0.930
486	Norton County, Kansas	Red Willow County, Nebraska	0.930
487	Hidalgo County, Texas	Kenedy County, Texas	0.930
488	Gilmer County, West Virginia	Lewis County, West Virginia	0.929
489	Choctaw County, Alabama	Marengo County, Alabama	0.929
490	Collier County, Florida	Monroe County, Florida	0.929
491	Ben Hill County, Georgia	Telfair County, Georgia	0.929
492	Hartley County, Texas	Potter County, Texas	0.928

493	Claiborne County, Tennessee	Grainger County, Tennessee	0.928
494	Pike County, Georgia	Upson County, Georgia	0.928
495	Montgomery County, North Carolina	Richmond County, North Carolina	0.928
496	Fayette County, West Virginia	Summers County, West Virginia	0.928
497	Jefferson County, Arkansas	Lincoln County, Arkansas	0.928
498	Hickman County, Tennessee	Maury County, Tennessee	0.928
499	Grays Harbor County, Washington	Jefferson County, Washington	0.928
500	Anne Arundel County, Maryland	Prince George's County, Maryland	0.927
501	Irion County, Texas	Tom Green County, Texas	0.927
502	Catron County, New Mexico	Sierra County, New Mexico	0.927
503	Cumberland County, Tennessee	Morgan County, Tennessee	0.927
504	Pendleton County, West Virginia	Randolph County, West Virginia	0.927
505	Bollinger County, Missouri	Wayne County, Missouri	0.926
506	Bryan County, Georgia	Liberty County, Georgia	0.926
507	La Paz County, Arizona	Imperial County, California	0.926
508	Carson County, Texas	Donley County, Texas	0.926
509	Emanuel County, Georgia	Johnson County, Georgia	0.926
510	Claiborne County, Tennessee	Union County, Tennessee	0.926
511	Anderson County, Tennessee	Campbell County, Tennessee	0.925
512	Benson County, North Dakota	Eddy County, North Dakota	0.925
513	Anderson County, Texas	Henderson County, Texas	0.925
514	Adams County, Wisconsin	Portage County, Wisconsin	0.925
515	Floyd County, Virginia	Pulaski County, Virginia	0.925
516	Lee County, Arkansas	Phillips County, Arkansas	0.925
517	Richland County, Montana	McKenzie County, North Dakota	0.925
518	Alleghany County, Virginia	Botetourt County, Virginia	0.925
519	Jackson County, Kansas	Nemaha County, Kansas	0.924
520	Harrison County, Kentucky	Nicholas County, Kentucky	0.924
521	Clarke County, Alabama	Wilcox County, Alabama	0.924
522	Baker County, Georgia	Miller County, Georgia	0.924
523	Brown County, South Dakota	McPherson County, South Dakota	0.924
524	Douglas County, Colorado	Teller County, Colorado	0.924
525	Hamblen County, Tennessee	Jefferson County, Tennessee	0.924
526	Gratiot County, Michigan	Isabella County, Michigan	0.924
527	Bourbon County, Kentucky	Nicholas County, Kentucky	0.924
528	Craig County, Virginia	Giles County, Virginia	0.924
529	Hardeman County, Tennessee	McNairy County, Tennessee	0.924
530	Beaufort County, South Carolina	Colleton County, South Carolina	0.923

531	Calvert County, Maryland	Prince George's County, Maryland	0.923
532	Eastland County, Texas	Erath County, Texas	0.923
533	Franklin County, Illinois	Jefferson County, Illinois	0.923
534	Dale County, Alabama	Houston County, Alabama	0.923
535	Calhoun County, Mississippi	Grenada County, Mississippi	0.922
536	Caroline County, Maryland	Talbot County, Maryland	0.922
537	Logan County, West Virginia	Wyoming County, West Virginia	0.921
538	Maries County, Missouri	Osage County, Missouri	0.921
539	Grant County, West Virginia	Tucker County, West Virginia	0.921
540	Carroll County, Arkansas	Newton County, Arkansas	0.921
541	Macon County, Illinois	Moultrie County, Illinois	0.921
542	Allen Parish, Louisiana	Evangeline Parish, Louisiana	0.921
543	Hart County, Kentucky	Larue County, Kentucky	0.921
544	Dewey County, Oklahoma	Roger Mills County, Oklahoma	0.920
545	Creek County, Oklahoma	Osage County, Oklahoma	0.920
546	Jefferson County, Oregon	Marion County, Oregon	0.920
547	Randolph County, Alabama	Carroll County, Georgia	0.919
548	Carroll County, Missouri	Ray County, Missouri	0.919
549	Cedar County, Iowa	Scott County, Iowa	0.919
550	Baker County, Florida	Nassau County, Florida	0.919
551	DeKalb County, Indiana	LaGrange County, Indiana	0.919
552	Hancock County, Mississippi	Harrison County, Mississippi	0.919
553	Pecos County, Texas	Ward County, Texas	0.919
554	Trinity County, Texas	Walker County, Texas	0.919
555	Lafayette County, Arkansas	Bossier Parish, Louisiana	0.917
556	Owyhee County, Idaho	Humboldt County, Nevada	0.917
557	Lincoln County, Nevada	Nye County, Nevada	0.917
558	Grand County, Colorado	Larimer County, Colorado	0.917
559	Smyth County, Virginia	Wythe County, Virginia	0.917
560	Jasper County, Iowa	Tama County, Iowa	0.917
561	Campbell County, South Dakota	Walworth County, South Dakota	0.916
562	Floyd County, Kentucky	Pike County, Kentucky	0.916
563	Cherokee County, Georgia	Gordon County, Georgia	0.916
564	Marion County, Kentucky	Nelson County, Kentucky	0.915
565	Hill County, Montana	Liberty County, Montana	0.915
566	Bracken County, Kentucky	Pendleton County, Kentucky	0.915
567	Lewis County, New York	Oswego County, New York	0.914
568	Elko County, Nevada	Box Elder County, Utah	0.914

569	Estill County, Kentucky	Madison County, Kentucky	0.914
570	McDonald County, Missouri	Delaware County, Oklahoma	0.914
571	Buchanan County, Iowa	Delaware County, Iowa	0.914
572	Hart County, Georgia	Madison County, Georgia	0.914
573	Desha County, Arkansas	Bolivar County, Mississippi	0.914
574	Lincoln County, Wisconsin	Taylor County, Wisconsin	0.914
575	Kemper County, Mississippi	Lauderdale County, Mississippi	0.913
576	Adams County, Indiana	Van Wert County, Ohio	0.913
577	Boundary County, Idaho	Pend Oreille County, Washington	0.913
578	Baker County, Florida	Duval County, Florida	0.913
579	Dubois County, Indiana	Perry County, Indiana	0.912
580	Kane County, Utah	San Juan County, Utah	0.912
581	Catahoula Parish, Louisiana	Franklin Parish, Louisiana	0.912
582	Douglas County, Missouri	Ozark County, Missouri	0.912
583	Cumberland County, Tennessee	Roane County, Tennessee	0.912
584	Bledsoe County, Tennessee	Sequatchie County, Tennessee	0.911
585	Hampshire County, West Virginia	Morgan County, West Virginia	0.911
586	Daviess County, Missouri	DeKalb County, Missouri	0.911
587	Floyd County, Kentucky	Magoffin County, Kentucky	0.911
588	Crawford County, Kansas	Barton County, Missouri	0.911
589	Henderson County, Tennessee	Madison County, Tennessee	0.911
590	Brown County, Texas	San Saba County, Texas	0.911
591	Greenlee County, Arizona	Catron County, New Mexico	0.911
592	Humboldt County, Nevada	Pershing County, Nevada	0.911
593	Carter County, Missouri	Shannon County, Missouri	0.911
594	Bibb County, Georgia	Peach County, Georgia	0.910
595	Johnson County, Illinois	Saline County, Illinois	0.910
596	Dixon County, Nebraska	Clay County, South Dakota	0.910
597	Christian County, Kentucky	Muhlenberg County, Kentucky	0.910
598	Clark County, Wisconsin	Eau Claire County, Wisconsin	0.910
599	Rankin County, Mississippi	Smith County, Mississippi	0.909
600	Randolph County, West Virginia	Upshur County, West Virginia	0.909
601	Lycoming County, Pennsylvania	Union County, Pennsylvania	0.909
602	Mingo County, West Virginia	Wyoming County, West Virginia	0.909
603	Nueces County, Texas	San Patricio County, Texas	0.908
604	Lassen County, California	Shasta County, California	0.908
605	Quitman County, Georgia	Randolph County, Georgia	0.908
606	Desha County, Arkansas	Lincoln County, Arkansas	0.908

607	Marshall County, Minnesota	Grand Forks County, North Dakota	0.908
608	Oregon County, Missouri	Ripley County, Missouri	0.907
609	Lafayette County, Mississippi	Yalobusha County, Mississippi	0.907
610	Ochiltree County, Texas	Roberts County, Texas	0.907
611	Rockingham County, Virginia	Pendleton County, West Virginia	0.907
612	Grand County, Utah	Wayne County, Utah	0.907
613	Marshall County, Iowa	Tama County, Iowa	0.906
614	Adams County, Wisconsin	Sauk County, Wisconsin	0.906
615	Marion County, Arkansas	Taney County, Missouri	0.906
616	Concho County, Texas	Runnels County, Texas	0.906
617	Lyon County, Iowa	Minnehaha County, South Dakota	0.906
618	Custer County, Colorado	Huerfano County, Colorado	0.906
619	Crowley County, Colorado	El Paso County, Colorado	0.906
620	Phelps County, Missouri	Pulaski County, Missouri	0.906
621	Baker County, Georgia	Calhoun County, Georgia	0.905
622	Newaygo County, Michigan	Oceana County, Michigan	0.905
623	Harlan County, Kentucky	Perry County, Kentucky	0.905
624	Lamar County, Georgia	Monroe County, Georgia	0.905
625	Custer County, Colorado	Pueblo County, Colorado	0.904
626	Fergus County, Montana	Musselshell County, Montana	0.904
627	Bailey County, Texas	Hockley County, Texas	0.904
628	Itawamba County, Mississippi	Prentiss County, Mississippi	0.904
629	Floyd County, Georgia	Polk County, Georgia	0.904
630	Conway County, Arkansas	Pope County, Arkansas	0.903
631	Emanuel County, Georgia	Toombs County, Georgia	0.903
632	Wibaux County, Montana	McKenzie County, North Dakota	0.903
633	Gilmer County, Georgia	Lumpkin County, Georgia	0.903
634	Polk County, Florida	Sumter County, Florida	0.903
635	Clinton County, Illinois	Marion County, Illinois	0.902
636	Grant County, Arkansas	Saline County, Arkansas	0.902
637	Monongalia County, West Virginia	Preston County, West Virginia	0.901
638	Sumter County, Alabama	Kemper County, Mississippi	0.901
639	Geary County, Kansas	Riley County, Kansas	0.901
640	Cooper County, Missouri	Morgan County, Missouri	0.901
641	Juneau County, Wisconsin	Vernon County, Wisconsin	0.901
642	Essex County, Virginia	Richmond County, Virginia	0.900
643	Hamilton County, Illinois	Saline County, Illinois	0.900
644	Kenedy County, Texas	Willacy County, Texas	0.900

645	Monroe County, Ohio	Tyler County, West Virginia	0.900
646	Jackson Parish, Louisiana	Ouachita Parish, Louisiana	0.900
647	Chaves County, New Mexico	Lincoln County, New Mexico	0.900
648	Cuming County, Nebraska	Dodge County, Nebraska	0.899
649	Davis County, Iowa	Wapello County, Iowa	0.899
650	Carter County, Montana	Butte County, South Dakota	0.899
651	Franklin Parish, Louisiana	Richland Parish, Louisiana	0.899
652	Crittenden County, Arkansas	Lee County, Arkansas	0.898
653	Kemper County, Mississippi	Winston County, Mississippi	0.898
654	Franklin County, Illinois	Jackson County, Illinois	0.897
655	Chambers County, Alabama	Harris County, Georgia	0.897
656	Boone County, West Virginia	Wyoming County, West Virginia	0.897
657	Crane County, Texas	Pecos County, Texas	0.897
658	Berkshire County, Massachusetts	Rensselaer County, New York	0.897
659	Hampton County, South Carolina	Jasper County, South Carolina	0.896
660	Fulton County, Kentucky	Weakley County, Tennessee	0.896
661	Jim Wells County, Texas	San Patricio County, Texas	0.896
662	Chatham County, Georgia	Effingham County, Georgia	0.896
663	Fayette County, Alabama	Walker County, Alabama	0.895
664	Beaver County, Oklahoma	Ellis County, Oklahoma	0.895
665	Camden County, Missouri	Morgan County, Missouri	0.895
666	Franklin County, North Carolina	Warren County, North Carolina	0.895
667	Brazos County, Texas	Leon County, Texas	0.895
668	Idaho County, Idaho	Missoula County, Montana	0.895
669	Cascade County, Montana	Chouteau County, Montana	0.895
670	Jackson County, Colorado	Albany County, Wyoming	0.895
671	Benton County, Arkansas	McDonald County, Missouri	0.894
672	Bacon County, Georgia	Ware County, Georgia	0.894
673	Lake County, Montana	Missoula County, Montana	0.894
674	Montgomery County, Arkansas	Pike County, Arkansas	0.894
675	Franklin County, Indiana	Ripley County, Indiana	0.894
676	Christian County, Illinois	Shelby County, Illinois	0.894
677	Logan County, Colorado	Kimball County, Nebraska	0.894
678	Pickens County, Alabama	Noxubee County, Mississippi	0.894
679	Scott County, Minnesota	Sibley County, Minnesota	0.893
680	Clay County, Minnesota	Richland County, North Dakota	0.893
681	Claiborne Parish, Louisiana	Union Parish, Louisiana	0.893
682	Custer County, Oklahoma	Roger Mills County, Oklahoma	0.893

683	Aurora County, South Dakota	Davison County, South Dakota	0.893
684	Jasper County, Iowa	Poweshiek County, Iowa	0.893
685	Madison County, Georgia	Oglethorpe County, Georgia	0.892
686	Marion County, Florida	Putnam County, Florida	0.892
687	Jackson Parish, Louisiana	Lincoln Parish, Louisiana	0.892
688	Henry County, Missouri	Johnson County, Missouri	0.892
689	Fleming County, Kentucky	Nicholas County, Kentucky	0.892
690	Lee County, Texas	Milam County, Texas	0.891
691	Swain County, North Carolina	Cocke County, Tennessee	0.890
692	Humboldt County, Nevada	Malheur County, Oregon	0.890
693	Calhoun County, South Carolina	Clarendon County, South Carolina	0.890
694	Lucas County, Iowa	Monroe County, Iowa	0.890
695	Emmons County, North Dakota	Morton County, North Dakota	0.890
696	East Feliciana Parish, Louisiana	Saint Helena Parish, Louisiana	0.890
697	Allen Parish, Louisiana	Rapides Parish, Louisiana	0.890
698	Jefferson County, Iowa	Wapello County, Iowa	0.889
699	Treutlen County, Georgia	Wheeler County, Georgia	0.889
700	Bell County, Texas	Williamson County, Texas	0.889
701	Archer County, Texas	Wichita County, Texas	0.889
702	Angelina County, Texas	Trinity County, Texas	0.888
703	Harrison County, Ohio	Tuscarawas County, Ohio	0.888
704	Crockett County, Tennessee	Lauderdale County, Tennessee	0.888
705	Fayette County, Pennsylvania	Somerset County, Pennsylvania	0.888
706	Crittenden County, Arkansas	Saint Francis County, Arkansas	0.887
707	Anderson County, Texas	Leon County, Texas	0.887
708	Muhlenberg County, Kentucky	Todd County, Kentucky	0.887
709	Adair County, Missouri	Schuyler County, Missouri	0.887
710	La Paz County, Arizona	Maricopa County, Arizona	0.886
711	Itawamba County, Mississippi	Monroe County, Mississippi	0.886
712	Cerro Gordo County, Iowa	Mitchell County, Iowa	0.886
713	Sussex County, Delaware	Wicomico County, Maryland	0.886
714	Arkansas County, Arkansas	Monroe County, Arkansas	0.885
715	San Augustine County, Texas	Shelby County, Texas	0.885
716	Boyle County, Kentucky	Lincoln County, Kentucky	0.885
717	Caldwell County, Kentucky	Lyon County, Kentucky	0.885
718	Mason County, Michigan	Oceana County, Michigan	0.885
719	Leon County, Texas	Madison County, Texas	0.885
720	Highland County, Virginia	Pendleton County, West Virginia	0.885

721	Vermillion County, Indiana	Warren County, Indiana	0.884
722	Morgan County, Ohio	Muskingum County, Ohio	0.884
723	Brown County, Illinois	Morgan County, Illinois	0.883
724	Davison County, South Dakota	Douglas County, South Dakota	0.883
725	Cross County, Arkansas	Saint Francis County, Arkansas	0.883
726	Reeves County, Texas	Ward County, Texas	0.883
727	Benton County, Tennessee	Houston County, Tennessee	0.883
728	Placer County, California	Yuba County, California	0.882
729	Chippewa County, Wisconsin	Taylor County, Wisconsin	0.882
730	Whitley County, Kentucky	Campbell County, Tennessee	0.882
731	Marshall County, Iowa	Poweshiek County, Iowa	0.882

TABLE S1. Reported spatial disparities in lung cancer mortality between neighbouring US counties.

REFERENCES

- RStan: The R interface to Stan. Stan Development Team, 2023.
- A. Datta, S. Banerjee, J. S. Hodges, and L. Gao. Spatial disease mapping using directed acyclic graph auto-regressive (DAGAR) models. *Bayesian analysis*, 14(4):1221, 2019.
- L. Gao, S. Banerjee, and B. Ritz. Spatial Difference Boundary Detection for Multiple Outcomes Using Bayesian Disease Mapping. *Biostatistics*, 24(4):922–944, Oct. 2023. ISSN 1465-4644. doi: 10.1093/biostatistics/kxac013.
- P. Li, S. Banerjee, T. A. Hanson, and A. M. McBean. Bayesian models for detecting difference boundaries in areal data. *Statistica Sinica*, 25(1):385, 2015.